Renewable Energy xxx (2018) 1–17

Contents lists available at ScienceDirect

Renewable Energy

journal homepage: www.elsevier.com/locate/renene

Reactivity controlled compression ignition and low temperature combustion of Fischer-Tropsch Fuel Blended with n-butanol

Valentin Soloiu*, Remi Gaubert, Jose Moncada, Justin Wiley, Johnnie Williams, Spencer Harp, Marcel Ilie, Gustavo Molina, David Mothershed

Department of Mechanical Engineering, Georgia Southern University, Statesboro, GA 30460, United States

ARTICLE INFO

Article history:
Received 23 February 2018
Received in revised form
6 August 2018
Accepted 15 September 2018
Available online xxx

Keywords:
Reactivity controlled compression ignition
n-Butanol
Gas to liquid kerosene
Low temperature combustion
Ringing
Emissions

ABSTRACT

LTC was researched by introducing an 80% mass fraction of n-butanol in reactivity controlled compression ignition (RCCI) mode. A 60% mass fraction of n-butanol was port fuel injected (PFI) and the additional 20% was directly injected through a blend of n-butanol (Bu) with Fischer-Tropsch gas to liquid synthetic paraffinic kerosene (GTL) or ULSD as reference. The blended fuels GTL20-Bu80 and ULSD20-Bu80 have reduced cetane for improved combustion phasing control compared to the reference RCCI mode with direct injection of neat ULSD and n-Butanol PFI (ULSD40-Bu60). RCCI strategies delayed ignition and increased peak heat release rates due to prolonged mixing time and reactivity stratification, inducing faster flame speeds. In RCCI mode, the ringing intensity (RI) increased up to 85% higher than in CDC. NOx and soot were reduced up to 90% with ULSD40-Bu60 compared to CDC. The butanol blends decreased CO by 25% compared to ULSD RCCI. CO levels overlayed each other for GTL20-Bu80 and ULSD20-Bu80 across loads, suggesting that the butanol was the influencing factor. ULSD and ULSD20-Bu80 RCCI increased mechanical efficiencies compared to CDC by 3–4% across loads. ULSD20-Bu80 had the lowest cetane and displayed the greatest improvement in the overall emissions and efficiencies in RCCI compared to CDC.

1. Introduction

Diesel engines are widely used in transportation, power generation, and construction given their high torque output, durability, high fuel efficiency, and ability to operate within a wide range of fuels and conditions [1]. The engines produce emissions, which are sources of harmful pollutants that have adverse effects on human health and the environment. Advanced combustion strategies have been developed to address emissions formation in-cylinder to meet increasingly stringent emissions regulations without the use of after treatment systems. These strategies have the potential to achieve low temperature combustion (LTC) and are capable of reducing both nitrogen oxides (NOx) and particulate matter (PM) simultaneously [2–11]. Common LTC approaches are identified as Homogenous Charge Compression Ignition (HCCI) and Premixed Charge Compression Ignition (PCCI). These strategies are limited to a range of loads and rely on high levels of exhaust gas recirculation (EGR) at high load operating points to increase ignition delay and avoid engine instability and knock. For improved control of the heat release rate and a wider range of operating loads, Reactivity Controlled Compression Ignition (RCCI) has been developed through dual fuel combustion with multiple injection events. Usually, RCCI implements an early port fuel injection (PFI) of low reactivity fuel, such as gasoline or an alcohol derived fuel, and split direct injections of high reactivity fuel, such as ultra-low sulfur diesel (ULSD). Multiple injection events coupled with two fuels of differing ignition qualities creates reactivity gradients with variances in local equivalence ratios for a gradual heat release rate and control of the ignition timing.

The majority of RCCI research has covered gasoline, propane, and compressed natural gas as the low reactivity fuel coupled with ULSD as the high reactivity fuel; however, there is a lack of research with n-butanol and Fischer Tropsch fuels in RCCI studies. The low reactivity fuel in this research was n-butanol, given its potential as a sustainable and renewable fuel along with its ability to mix with ULSD and kerosene without phase separation [12]. n-Butanol is an oxygenate obtained from non-food sources and agricultural waste

* Corresponding author. Georgia Southern University, 201 COBA Drive, Statesboro, GA, 30458, United States.
E-mail address: vsoloiu@georgiasouthern.edu (V. Soloiu).

https://doi.org/10.1016/j.renene.2018.09.047
0960-1481/

as well as from the same feedstock used in ethanol production [13–15]. This is advantageous since the strong moisture-absorption of ethanol becomes an issue when blended with gasoline [8]. Additionally, this long-chain alcohol has desirable combustion characteristics such as a high calorific value, low water absorption, low-corrosivity in to pipelines, and better miscibility with ULSD compared to methanol and ethanol [11]. The methods to produce bio-derived n-butanol have thus been more prevalent [16]. The fuels in the common rail for this research included neat ULSD, a 50% by mass blend of butanol and ULSD, and a 50% by mass blend of butanol and gas to liquid kerosene (GTL). These three fuels have varying ignition qualities, creating a cetane number parametric study. GTL was evaluated as a Fischer Tropsch (F-T) fuel which is a potential alternative for the traditional petroleum derived fuels. These fuels offer a sustainable alternative and can be produced from various carbon based resources such as natural gas, coal, or biomass. F-T fuels typically contain little to no aromatics, are more volatile, have higher H/C ratios, and a higher heat of vaporization compared to ULSD [17]. F-T fuels are also attractive alternatives to diesel, as they are cleaner fuels capable of reducing exhaust emissions. Moreover, the production process has become highly efficient. Through the derivation from various sources, F-T fuels can potentially decentralize energy resources, improving the stability of world energy markets [18]. As a reference for comparison with RCCI, combustion with single fuel direct injection of diesel was used to perform conventional diesel combustion (CDC) with maintained combustion phasing.

Fuel lubricity is important as it can be damaging to tight tolerance parts such as the high pressure rotary pump and common rail fuel injector. The lubricity characteristics of butanol-diesel blends were investigated by Ref. [8], where it was found that blends with more than 20% butanol did not meet diesel fuel specifications. However, with only 2% biodiesel, wear scar diameter results were in the range of neat diesel. Jet fuels, such as GTL, also have low lubricity characteristics as commercial jet fuel does not have a specific lubricity requirement and require lubricity additives for military use [19]. F-T fuels have been found to result in acceptable high frequency reciprocating rig results with only 1% biodiesel [20]. For these reasons, both the ULSD and GTL n-butanol blends were mixed with 3% by volume of biodiesel to maintain the lubrication characteristics.

2. Literature review

2.1. Dual fuel combustion with n-Butanol

Han et al. [4] investigated RCCI combustion with 40%–75% PFI of n-butanol in a 0.5 L single cylinder engine at 1500 RPM and 8 bar indicated mean effective pressure (IMEP). With 40% PFI and late DI timing near top dead centre (TDC), the butanol begins to auto ignite, and is extinguished due to the diesel injection resulting in a two stage heat release as also reported by Soloiu et al. [5]. Combustion phasing control was comparable to that of conventional diesel HTC, however, this resulted in significant diffusion burning. Higher ratios of n-butanol helped reduce NOx emissions at lower EGR ratios. Soot emissions, however, showed minor changes with increased butanol fractions and resulted in levels higher than those in PCCI and HCCI modes.

Wang et al. [7] researched RCCI comparing PFI of n-butanol to LTC gasoline in a 2.44 L engine, at 1300 RPM and 6.5 and 9.0 bar IMEP. At 6.5 bar, the increased fuel requirement of diesel in the butanol case shortened combustion duration and lowered pressure rise rates compared to gasoline. At swept intake pressures, butanol RCCI resulted in lower unburned hydrocarbon (UHC) emissions, maximum pressure rise rates, and comparable combustion efficiency to gasoline RCCI, however, carbon monoxide (CO) emissions increased and thermal efficiencies decreased. At 9.0 bar IMEP, RCCI with butanol had lower soot and pressure rise rates compared to gasoline RCCI and higher gross thermal efficiency.

Michikawauchi et al. [8] researched dual combustion of n-butanol by blending with ULSD and by PFI of the butanol in a 2.2 L four cylinder engine. At high load and 30% butanol, NO_x was reduced for both the PFI and blending method by 43% and 40% respectively, and by 73% and 50% at mid load. NO_x reduction was larger when increasing the ratio of butanol for the PFI method compared to the blending method. These results are due to the increase in the ratio of premixed combustion caused by higher quantities of butanol-air mixture and the butanol's cooling effect. Butanol did, however, reduce thermal efficiencies due to higher UHC emissions. Soot emissions were further reduced by the blended fuel than PFI of butanol due to the post injection also containing butanol promoting higher rates of soot oxidation.

Nayyar et al. [21] performed research at 1500 rpm across loads from part to full load in a 3.75 kW single cylinder CI engine. Butanol-diesel blends were compared at 10%, 20%, and 25% butanol. Decreases in smoke emissions consistently reduced with the increased ratio of butanol because of the increased oxygen in fuel-rich regions. NO_x emissions were reduced at 10% and 20% blends and increased at a blend of 25%. At the two lower blend ratios, the extended ignition delay compared to neat ULSD increased the mixing time and reduced combustion temperature due to the high latent heat of vaporization of butanol. The improved combustion from increased mixing time was also found to reduce combustion duration from improved flame speed. However, the 25% blend overextended ignition delay causing higher peak heat release rates and temperatures. Brake thermal efficiencies (BTE) followed a similar trend to NOx, where BTE increased for the 10% and 20% blends, however, reduced for the 25% blend from too long of an ignition delay and reduced mean effective pressure.

2.2. Combustion characteristics of Fischer Tropsch fuels

Soloiu et al. [5] researched partially premixed compression ignition (PPCI) combustion coupling direct injected F-T GTL with 30% port fuel injected n-butanol compared to ULSD with n-butanol in a 1.1 L experimental diesel engine. A late direct injected event delayed the high temperature heat release. Peak heat release rates and maximum pressure rise rates were reduced for GTL-PPCI compared to ULSD-PPCI due to reduced ignition delay. NO_x levels were reduced by 25% across three engine loads, where soot and CO increased at the highest load, which is attributed to undermixing. Reduced UHC levels were also reported with GTL from less wall wetting of the lower density fuel.

Atkinson et al. [22] evaluated F-T Fuels in 7.3 L heavy duty diesel engine. These fuels have high ignition quality and near zero sulfur content. The high cetane number and lower density compared to diesel has been determined to decrease ignition delay, lower peak heat release rates, and combustion duration. The reduction in mixing time directly causes an average capability of reducing NO_x by 20% and particulate matter by 31%. NO_x reductions were observed from the reduction in the premixed burn duration. However, combustion duration was extended from the less prominent premixed burn resulting in a slower burn rate. Overall, F-T fuel was found to reduce all regulated emissions, apart from UHC at some speeds and loads.

Kitano et al. [23] compared two GTL fuels, (A) with a cetane number of 85.2 and comparable distillation range to diesel and (B) a cetane number of 71.5 with a lower distillation range, compared to diesel fuel in a 2.0 L four cylinder engine. NO_x emissions were not significantly affected by either GTL fuels due to the small impact on

Please cite this article in press as: V. Soloiu, et al., Reactivity controlled compression ignition and low temperature combustion of Fischer-Tropsch Fuel Blended with n-butanol, Renewable Energy (2018), https://doi.org/10.1016/j.renene.2018.09.047

combustion temperature. The GTL fuel improved PM, UHC, and CO emissions along with reduced engine noise due to the shorter ignition delay. GTL B had a lower distillation temperature than GTL A, which further reduced PM due to the increased volatility with the air mixture. Higher ignition quality at low temperature was found to attribute to the reduced UHC levels, given that the fuel has a higher tendency to react. A disadvantage of GTL is the increased volumetric flow rate compared to diesel due to the lower density, where GTL A and GTL B increased this rate by 4.0% and 5.9% respectively.

Piperel et al. [24] investigated a single cylinder direct injected engine operating with a fuel blend containing 40% F-T GTL fuel by volume, neat F-T GTL fuel, and baseline ULSD. The engine was operated at 3 bar IMEP at 1500 RPM and at full load at 4000 RPM. Hydrocarbon and CO emissions reduced at low load with the GTL fuels but increased the ringing intensity from earlier combustion and higher heat release rates. GTL is more volatile and has a higher ignition quality than diesel, causing the increased heat release rate at shorter ignition delay periods. Smoke emissions decreased up to 34% with the GTL fuels at high load along with a 2% increase in maximum power. The reduced smoke emissions is attributed to the low aromatic content of GTL compared to diesel.

Abu-Jrai et al. [25] conducted a comparison of ULSD and F-T GTL fuel with a much higher cetane number than ULSD. The test was operated on a direct injected engine at 1200 and 1500 RPM at 25% and 50% of the engine's maximum torque. At various levels of EGR, it was found that engine efficiency was not as sensitive to increased EGR rates as compared to diesel. The higher cetane number for GTL fuel is the attributing factor to the lower sensitivity to EGR. It was also found that GTL had an earlier onset of combustion, reducing maximum pressure rise rates and heat release rates, where there is less fuel burned during the premixed phase. NOx and soot levels were reduced by 40% and 30% respectively with 10% reformed EGR compared to diesel. CO emissions, however, were found to increase, corresponding to the lower combustion temperatures for GTL.

3. Thermal and physical properties of research fuels

3.1. Fuel characteristics

Physiochemical properties analysis of the studied fuels was conducted given their significant impact on combustion phasing and emissions. These properties were obtained experimentally by the authors and are provided in Table 1. The analysis of the fuels includes an additive in the form of 3% by volume of biodiesel. This was added to n-butanol blends for increased lubricity which serves to protect the injection system.

Energy content of the fuels was determined with a Parr 1341 constant volume calorimeter (error 0.3%) for comparison of the potential fuel efficiencies. Considering the molecular composition of the fuels, the lower heating value (LHV) was determined, with ULSD having the highest energy content at 41.66 MJ/kg. The reduced butanol reactivity blends had similar LHV of about 38 MJ/kg, while neat n-butanol had an LHV of 33.7 MJ/kg. This value is 20% higher than ethanol, which can effectively result in improved fuel consumption [27]. The dynamic viscosity was then measured, as displayed in Fig. 1, given its effect on atomization, droplet speed, and spray penetration. This property was obtained with a Brookfield DV II Pro rotational viscometer operated with a spindle speed of 200 rpm. The measurements were taken at a temperature range from 26°C to 90 °C, with the GTL fuel blend showing the lowest viscosity. The ULSD blend viscosity curve did result in a cross over with the neat n-butanol curve at 38 °C.

The cetane number (DCN) of the fuels was derived with a CID510 constant volume combustion chamber from PAC. The instrument has a Bosch solenoid injector with a seven-hole nozzle, simulating the common rail system of modern diesel engine. The constant volume combustion chamber (CVCC) design is shown in Fig. 2 with the adjacent sensors and injection system. The CID510 is configured with a solenoid injector and pressure multiplier (1), a uniformly heated chamber (2), a chamber pressure sensor (3), and a fuel line pressure sensor (4). The DCN was obtained following ASTM method D7668-14a [28] which used a defined set of operating parameters. Measurements of ignition delay (ID) and combustion delay (Cd) were then derived using Eq. (1) from an average of 15 injection cycles. The ID defines the period from the start of injection (SOI) to the start of combustion (when pressure reached 22 bar in the

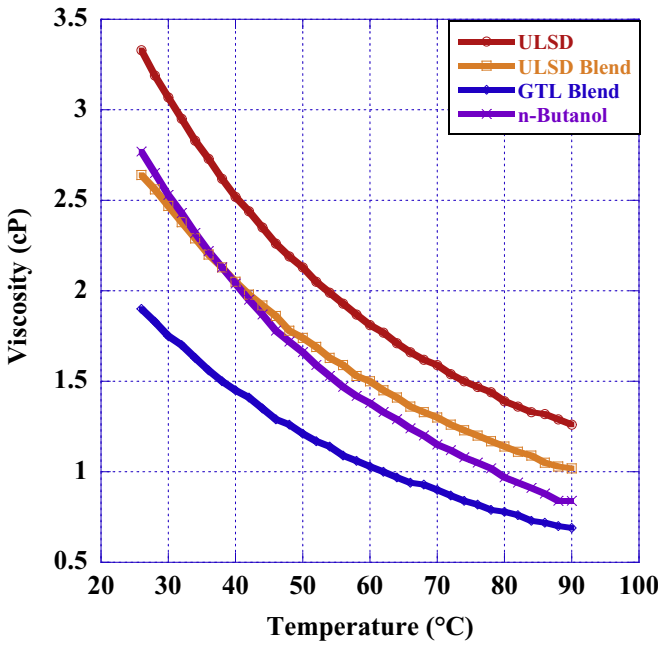

Fig. 1. Dynamic viscosity measurements.

Table 1
Selected fuel properties [b].

Properties	ULSD	F-T GTL POSF 5109	ULSD Blend	GTL Blend	n-Butanol
Density (g/cm^3) @ 15°C	0.84 g/cm^3	0.755 g/cm3	0.82 g/cm^3	0.783 g/cm^3	0.807 g/cm^3
Lower Heating Value	42.6 MJ/kg	41.5 MJ/kg	37.9 MJ/kg	37.8 MJ/kg	33.1 MJ/kg
Dynamic Viscosity @ 40°C	2.5 cP	1.09 cP	1.77 cP	1.45 cP	2.0 cP
DCN	47.2	61.58	28.2	34.3	16.4
Ignition Delay (CVCC)	3.47 ms	2.73 ms	7.97 ms	5.71 ms	40.16 ms
Combustion Delay (CVCC)	5.12 ms	3.93 ms	14.44 ms	9.12 ms	81.25 ms
Latent Heat of Vaporization	233 kJ/kg[a]	339 kJ/kg[a]	–	–	595 kJ/kg[a]

[a] Obtained from literature [26].
[b] Obtained by the authors of the study.

Please cite this article in press as: V. Soloiu, et al., Reactivity controlled compression ignition and low temperature combustion of Fischer-Tropsch Fuel Blended with n-butanol, Renewable Energy (2018), https://doi.org/10.1016/j.renene.2018.09.047

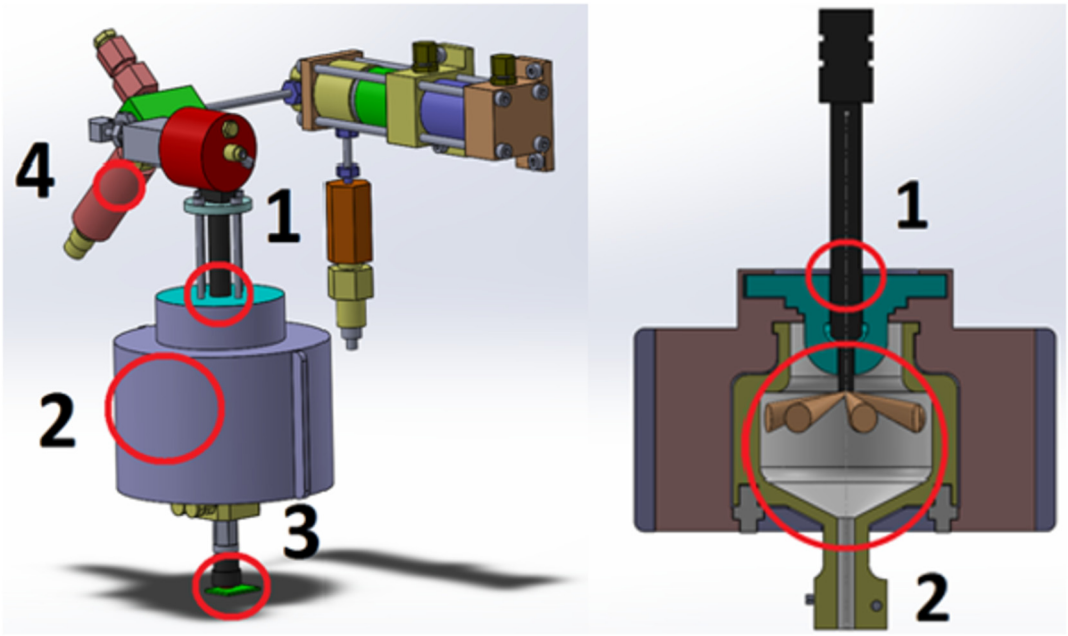

Fig. 2. CVCC design.

combustion chamber). The Cd is defined as the time from SOI to midpoint of the pressure curve. The operating parameters included the chamber being maintained at a 20 bar pressure and a 595 °C wall temperature while fuel was delivered at 1000 bar for 2.5 ms.

$$DCN = 13.028 - \frac{5.3378}{ID} + \frac{300.18}{Cd} + \frac{-1267.90}{Cd^2} + \frac{3415.32}{Cd^3} \quad (1)$$

Chamber pressures and heat release rates in the CVCC are illustrated in Fig. 3. Neat ULSD reached the highest pressure at 42 bar. Peak pressure for the two fuel blends had a peak pressure 1.5 bar lower than ULSD, being equal because of the same fuel energy content. ULSD had the highest DCN while the blends showed reduced values of 28.2 DCN for the ULSD blend and 34.3 DCN for the GTL blend. The reduction in autoignition quality is evident due to the low DCN of n-butanol. The neat n-butanol displayed a late combustion as seen in Fig. 3, igniting over 30 ms after the blends combust. The ignition delay for n-butanol was 40.16 ms, which is desirable for RCCI as it delays ignition and enhances combustion stability. ID and Cd were double for the ULSD blend and 1.5 times longer for the GTL blend compared to neat ULSD.

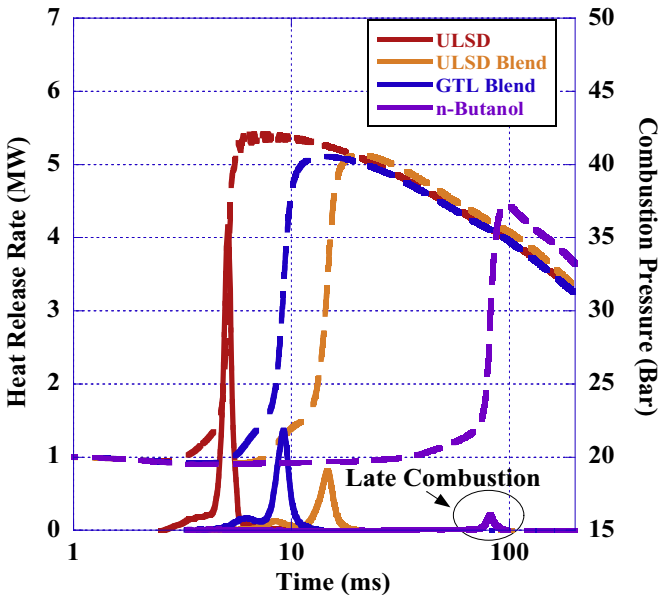

Fig. 3. Pressure and heat release rates in the CVCC.

Heat release rates were proportional to the pressure rise rate because of the constant volume combustion. The ULSD and GTL blends had lower peak heat release rates than neat ULSD by 80% and 65% respectively. The low reactivity of n-butanol is notable as it had a 95% lower maximum heat release rate than ULSD. Low temperature heat release can also be observed early in the combustion process, which is associated to a negative temperature coefficient (NTC) area. The NTC region, illustrated by magnifying the heat release rates as presented in Fig. 4, results from intermediate fuel oxidation paths where rates decrease due to the present ambient temperatures. The NTC region showed correlation with the fuel reactivity as the fuel with the greatest cetane number had the region with the highest magnitude and the shortest duration. The low temperature heat release and NTC region is thus more prominent for the blended fuels, which resulted in a lower high temperature heat release after ignition. n-Butanol additionally shows a slight low temperature heat release produced from a high latent heat of vaporization, enabling a cooling effect in the chamber. The related vaporization and energy release profile of the fuels was then analyzed with a thermogravimetric and a differential thermal analysis (TGA-DTA).

3.2. Low temperature heat release analysis by TGA-DTA

Thermogravimetric analysis and differential thermal analysis was conducted using a Shimadzu DTG-60 (accuracy of ±1.0 °C and ±1% error), which regulated a chamber with a constantly purged atmosphere and constant air flow at 15 mL/min. The fuel analysis was performed at increasing temperatures from 20 °C to 600 °C, where temperature increased at a rate 20 °C/min. The TGA measured the change in mass of the fuel as it vaporizes as shown in

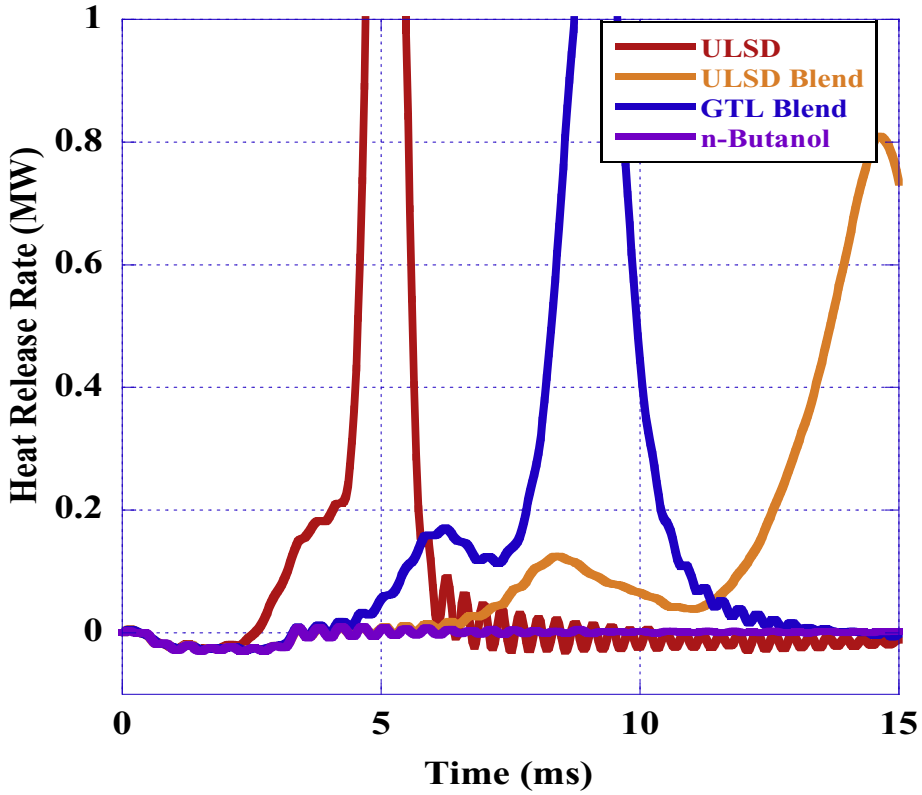

Fig. 4. Negative temperature coefficient region in the CVCC.

Fig. 5. The volatility in respect to temperature can be determined from the curve and correlate with mixing with the in-cylinder once the fuel vaporizes.

ULSD started vaporizing at 115 °C (TA10), while n-butanol was completely vaporized at the same temperature as presented in Table 2. The ULSD and GTL blends displayed a two stage vaporization curve where n-butanol content vaporized first followed by the vaporization of the high reactivity fuel. The temperatures at which 10%, 50%, and 90% of the mass of each fuel was vaporized (TA10, TA50, and TA90) are presented in Table 2. The lower vaporization temperatures compared to neat ULSD can be beneficial for avoiding wall wetting due to decreased spray penetration and earlier fuel-air mixing.

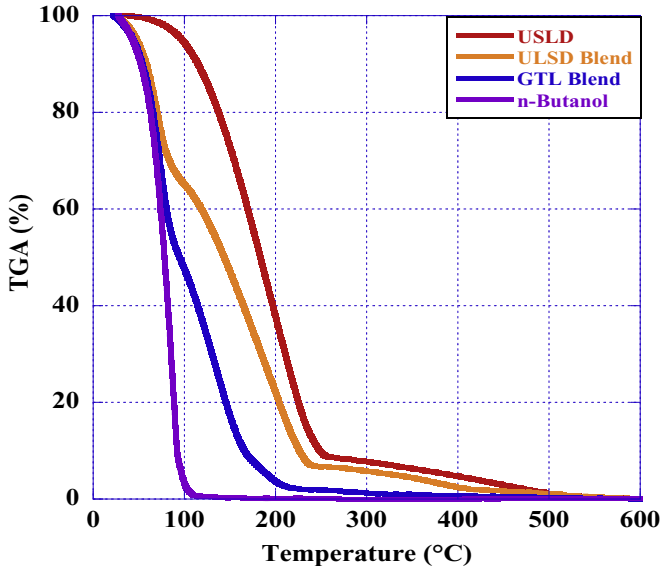

Fig. 5. Thermogravimetric analysis.

Table 2
TGA vaporization temperatures.

	TA10	TA50	TA90
ULSD	115 °C	185 °C	250 °C
ULSD Blend	58 °C	144 °C	226 °C
GTL Blend	54 °C	95 °C	166 °C
n-Butanol	52 °C	78 °C	92 °C

The DTA analysis measures the fuels' energy release. This represents the absorption and release of the heat in comparison to a reference baseline. The profile obtained with the DTA represented the low temperature heat release of each fuel as illustrated in Fig. 6. The concave curves represent the endothermic reactions while the convex curves correlate to the exothermic reactions. The heat release of the fuels can be categorized in three stages due to fuel vaporization, initial oxidation and final pyrolysis. The high latent heat of vaporization of n-butanol is apparent in the DTA curve where there is steep endothermic reaction around TA90. This is advantageous for creating a cooling effect in the cylinder and reduces peak combustion temperatures in the experimental engine. Correlating to the two-stage vaporization of the blends, the DTA for the blends showed an initial concave region demonstrating the heat absorption of the alcohol. The GTL blend had a steeper endothermic reaction at the same temperature compared to the ULSD blend, as a result of the higher heat of vaporization of GTL. A second concave region can be observed for GTL just before TA50, which is less gradual than that of ULSD. The magnitude of the fuel mass fraction remaining affected the rate of the pyrolysis reaction

Please cite this article in press as: V. Soloiu, et al., Reactivity controlled compression ignition and low temperature combustion of Fischer-Tropsch Fuel Blended with n-butanol, Renewable Energy (2018), https://doi.org/10.1016/j.renene.2018.09.047

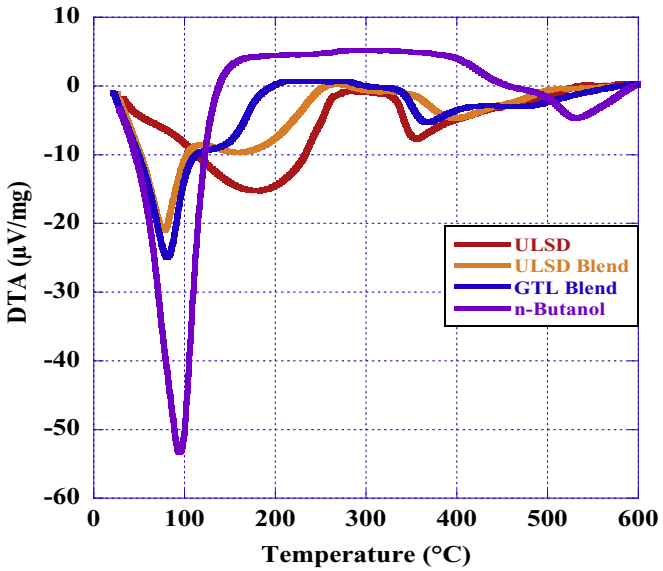

Fig. 6. Differential thermal analysis.

shown towards the end of the DTA curve.

3.3. MIE scattering spray analysis

The studied fuels were analyzed for their spray development and mixture formation using a Malvern He-Ne laser. It was found that different fuel densities and viscosities correlate with spray penetration during experimental engine operation [29]. The laser was part of an experimental system shown in Fig. 7, which interfaced with Spraytec Mie scattering software calculating spray volume distribution and Sauter Mean Diameter (SMD) following the standard BS 2955/1993. The experimental configuration consisted of a (1) transmitter which emits a laser with a 632.8 nm wavelength that is normalized by (2) collimating optics and sent it through the evaluated (3) spray droplets. The (4) focusing lens then capture the light that was not scattered from the beam into a Fourier arrangement that is captured by the detector elements. The detector collects how the light scatters based the range of particle diffraction angles. The fuel was delivered by a reference pintle tip injector which was placed 100 mm from the laser beam. The fuel was delivered at 180 bar on to room temperature and atmospheric pressure which serves as a control environment for comparative study between fuel properties. Neat n-butanol was not investigated as it was only port fuel injected.

Data was collected at 10 kHz for 5 ms from 0.1 ms before the injection triggered. The droplet distributions across the volume as well as the SMD over time are shown in Fig. 8 for neat ULSD and ULSD & GTL blends. The peak spray volume frequency showed that 35 μm was the most prominent droplet size across the volume for both the GTL blend and the neat ULSD at 7% and 8%, respectively. The peak frequency for the ULSD blend was 40 μm at 8% of the volume. The higher concentration of lower droplet sizes can be advantageous for lower spray velocities and penetration in the combustion chamber from the nozzle. The analysis also shows different boundary interaction with n-butanol between GTL and ULSD, which affected the overall SMD as provided in Table 3. The table also includes the droplet diameter for 10%, 50%, and 90% of the spray volume. Droplet sizes for the GTL blend across time display the lowest SMD values, with results for both ULSD and the ULSD

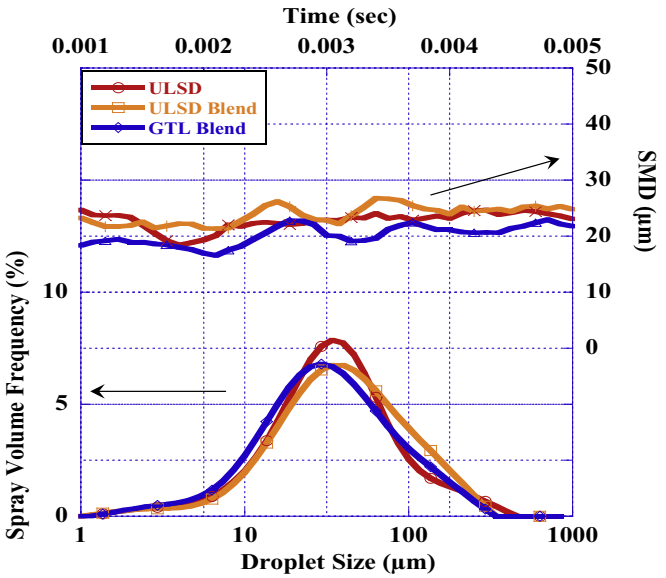

Fig. 8. Spray droplet distribution and SMD of selected fuels.

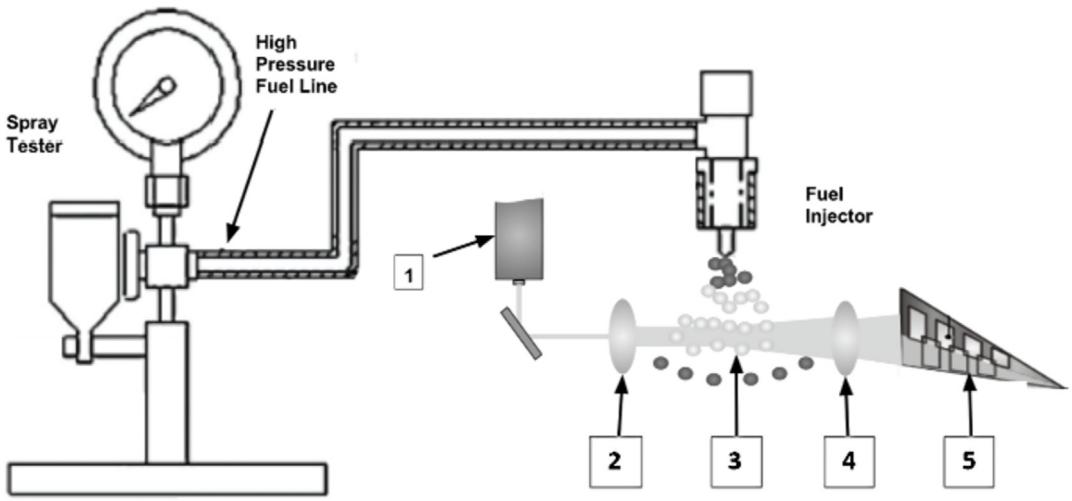

Fig. 7. MIE scattering Malvern laser - experimental configuration.

Please cite this article in press as: V. Soloiu, et al., Reactivity controlled compression ignition and low temperature combustion of Fischer-Tropsch Fuel Blended with n-butanol, Renewable Energy (2018), https://doi.org/10.1016/j.renene.2018.09.047

Table 3
Particle size distribution by volume (μm).

	Dv (10)	Dv (50)	Dv (90)	SMD	%v < 10 μm
ULSD	12.3	37.9	120.5	22.8	9.5
ULSD Blend	12.9	42.2	135.1	24.3	8.6
GTL Blend	10.5	34.4	116.6	20.8	12.2

Table 4
Experimental engine specs.

Bore x Stroke	112 mm × 115 mm
Number of Cylinders	1
Compression ratio	16:1
Displacement	1.132 L
Maximum Power	17 kW @ 2200 rpm
Maximum Torque	77.5 N m at 1400 RPM
Cooling System	Water
DI Injection Nozzle	7 × 0.115 mm
Rail Pressure	800–1200 bar
PFI Pressure	2.76 bar

blend being similar. Lower viscosity fuels typically have smaller droplet sizes, however the lower density of the ULSD blend reduces the force on the pintle injector affecting atomization.

4. Experimental engine setup

The research was conducted with a medium duty experimental diesel engine with a proprietary designed high pressure common rail system replacing the OEM injection system. The common rail is configured with an externally driven Bosch CP3 radial pump and piezoelectric fuel injector with a custom nozzle designed for the OEM combustion chamber. The nozzle has an asymmetric spray with a spray angle reducing from 85° to 50° for suitable propagation in the combustion chamber at the designed injection timing. The specifications for the experimental engine are included in Table 4. The engine was additionally implemented with a low-pressure EGR circuit, a PFI system, and a Procharger centrifugal supercharger driven by an external AC motor with a variable frequency drive as illustrated in Fig. 9. A National Instruments DI driver (NI 9751) and a PFI driver (NI 9758) were interfaced through a NI Compact Rio 9076 to control the common rail system and the port fuel injector, allowing for various strategies of operating parameters and combustion phasing (CA50). Engine speed and rail pressure were maintained by closed loop PID control.

A Kistler 6053 cc uncooled piezoelectric pressure transducer was used to collect the in-cylinder pressure in relation to crank angle measurements across the engine cycle averaging 100 cycles per operating point. The crankshaft positioning was obtained with an Omron E6C3-CWZ3EH incremental rotary encoder with a resolution of 3600 pulses per revolution collecting data at every 0.2 CAD or at every 22 μs. The pressure transducer was conditioned with a Kistler 5010B dual mode charge amplifier for measurements of cycles at 45 kHz using a Yokogawa DL850 high speed data acquisition system. The sensor was additionally coupled to AVL Indicom v2.5 for measuring stability of the engine combustion process, monitoring the coefficient of variation (COV) of the indicated mean effective pressure (IMEP) and CA50 during steady-state operation. The engine was operated across loads which were applied with a hydraulic dynamometer coupled to the crankshaft measuring brake power with a TQ513 series Omega torque cell.

Intake flow rates were measured with a Meriam Z50MC-2 laminar flow meter interfaced with a LFS-1 electronic measurement system. The meter had an adjacent sensor for temperature, pressure, and relative humidity for flow rates environmental corrections. The EGR rates were controlled with a back pressure valve at the exhaust manifold; the EGR percent was determined by the ratio of CO_2 in the intake to that in the exhaust as measured by two EMS Model 5002 exhaust gas analyzers. Recirculated exhaust gas temperatures were controlled with an EGR cooler, while maintaining temperatures above the dew point. An exhaust pressure sensor was used to control the available backpressure in the exhaust manifold.

Constant boost of 0.2 bar (3 psi) was maintained across the operated loads with pressure sensors measuring the boost pressure at the intake surge tank and intake pressure in the intake valve port. An Omega PX3030 and a Kulite ETL-175-190M pressure transducer were used to respectively measure the boost and intake. The intake additionally had in place PID-controlled heaters for maintaining the temperature at levels for adequate vaporization of the n-butanol. Fuel flow rate for direct injection was measured with Max

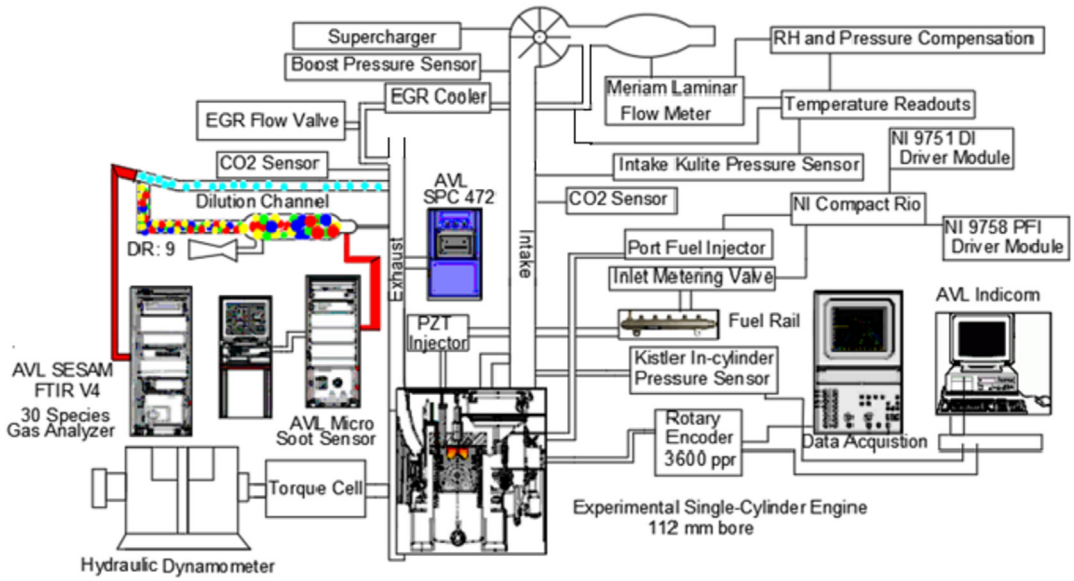

Fig. 9. Experimental Engine Setup [30].

Table 5
Measurement uncertainties.

NOx	3.13%
Soot	3.35%
CO	3.12%
UHC	3.32%
HCHO	3.11%
$P_{effective}$	2.90%
BSFC	2.89%

Machinery $P2_13$ piston flow meters while PFI flow rate was measured with a P001 model. The sampling rate was 1.25 MS/s for the fuel flow measurements when using an additional National Instruments DAQ. Gaseous emissions were measured with an AVL SESAM FTIR V4 using the default diesel recipe while particulate matter was measured with an AVL 483 Micro Soot Sensor at a rate of 1 Hz. The sampling lines were maintained at 191 °C to avoid condensation and carbon deposits.

Accuracies for selected instruments in the experimental engine setup are in included in Appendix A. The uncertainty on the brake specific emissions and fuel consumption was also calculated based on the collected measurements and the accuracy of the used sensors. These uncertainties are present due to calibration and atmospheric conditions varying the nominal measured values. The root sum square method was utilized to obtain the uncertainties shown in Table 5.

5. Experimental methods

The engine was operated across three loads from 4 to 6 bar IMEP at 1500 rpm, which was selected due to its proximity to the maximum brake torque of the experimental engine. The effects of the alternative fuels on combustion were investigated in RCCI mode compared to CDC. Equal parts blends by mass of n-butanol-ULSD (ULSD20-Bu80) and n-butanol-GTL (GTL20-Bu80) were researched as the high reactivity component in comparison to neat ULSD (ULSD40-Bu60) for operation in RCCI, along with a constant 60% PFI rate of n-butanol. Split DI events were used to induce reactivity gradients in-cylinder; the first DI injection (SOI-1) was maintained at 60 crank angle degrees (CAD) BTDC and the start of the second injection (SOI-2) was adjusted around TDC to maintain COV below 5%. DI pressures ranged from 800 to 1200 bar, increasing with load to improve soot control. The PFI timing was set at exhaust valve closing, 345 CAD BTDC in combustion, to prevent scavenging during valve overlap.

Parameters were initially optimized for ULSD40-Bu60 and maintained constant to analyze the fuel effect on combustion and emissions. The SOI-1 fraction was changed to maintain combustion phasing for a CA50 set at combustion TDC, which obtains gross indicated thermal efficiencies (ITE) up to 56%. Intake temperature was maintained constant at 60 °C for control of CO rates. EGR was increased from 20% at lower load to 30% at higher loads for adjustment of CA50. Table 6 details the control parameters used for operation in CDC and RCCI with different high reactivity fuels.

6. Combustion results and discussion

The resulting injection durations and mass fractions used for RCCI and CDC are provided in Table 7; the variations for each fuel are clear due to differences in reactivity and energy density. The mass fractions were obtained as a result of keeping CA50 at TDC. This will mark two distinct moments in the cylinder before and after the SOI-2. As such, the local equivalence ratio will change as more fuel is introduced.

Table 6
Operating parameters for CDC and RCCI.

	SOI CDC	SOI-1 RCCI	SOI-2 RCCI	EGR %	Rail Pressure
4 IMEP	21° BTDC	60° BTDC	5° ATDC	20%	800 bar
5 IMEP	22° BTDC	60° BTDC	2° ATDC	30%	1000 bar
6 IMEP	24° BTDC	60° BTDC	1° BTDC	30%	1200 bar

Table 7
Injection duration (ms) and Mass fraction of the first DI event (%).

	4 IMEP	5 IMEP	6 IMEP
CDC	0.715/-	0.760/-	0.840/-
ULSD40-Bu60	0.275/58%	0.250/51%	0.235/45%
ULSD20-Bu80	0.380/79%	0.350/73%	0.310/57%
GTL20-Bu80	0.345/68%	0.340/68%	0.320/57%

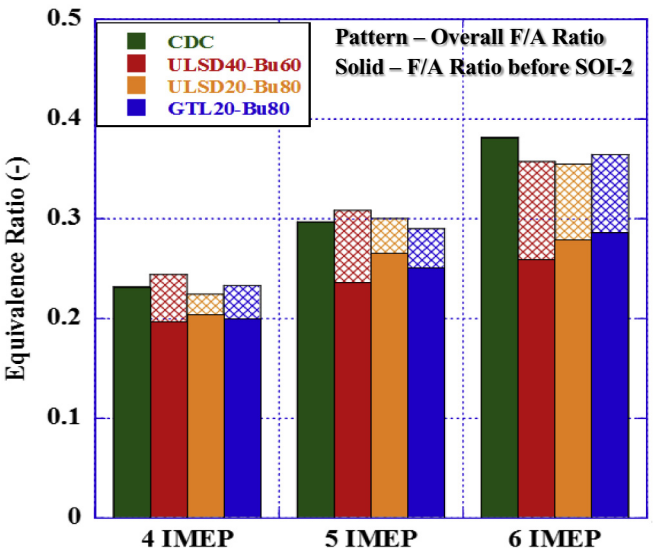

Fig. 10. Global equivalence ratios before and after SOI-2.

Fig. 10 details the values for the global equivalence ratio for each fuel before and after SOI-2. The equivalence ratio before SOI-2 provided further correlation with combustion characteristics as approximately half the combustion occurs before this injection event.

6.1. In-cylinder combustion pressure

Combustion pressures for RCCI and CDC operation are illustrated in Fig. 11 for the experimented loads. The delay in pressure rise is longer when comparing dual fuel combustion to CDC. The introduction of n-butanol through PFI extended the combustion event as observed in the CVCC. Initial pressure rise was delayed until 3 CAD BTDC with the indirect injected n-butanol. ULSD40-Bu60 had the same peak pressure as CDC while the GTL and ULSD blends increased peak pressure by 5–10 bar. The fuel amount in the cylinder increased at the time of premixed combustion as a result of increased SOI-1 mass fraction by 10–20% for the blended fueled RCCI compared to neat ULSD RCCI.

The ignition of the n-butanol in RCCI led to a sharper pressure rise to peak values. The fuel blends had a higher maximum pressure rise rate (MPRR) by 30–40% compared to ULSD40-Bu60. MPRR reached 15 bar/deg and 20 bar/deg (that correlates with the high ringing produced) for the butanol blends at 6 bar IMEP, which

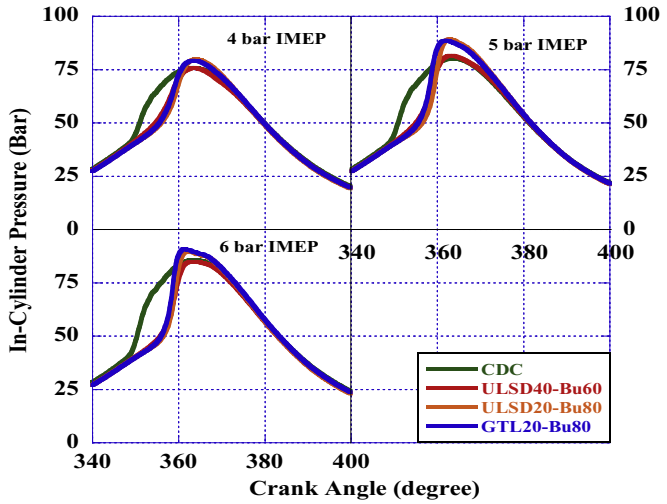

Fig. 11. In-Cylinder Pressure at 1500 rpm and 4, 5, and 6 bar IMEP.

exceeded the conventional limit of 15 bar/deg found in literature. In order to reduce the high levels of MPRR, combustion phasing could be delayed, however, this remained a controlled variable in order to study the fuel effects in RCCI. At 6 bar IMEP, an inflection can be observed at peak pressure (shown in more detail in Fig. 12), due to the cooling effect of n-butanol when introduced by SOI-2. This behavior can be attributed to the blended n-butanol as it is not seen for ULSD40-Bu60 at TDC (the red line).

6.2. Apparent heat release rate

The apparent heat release rate (AHRR) was obtained from the combustion pressures using a model as shown in Eq. (2) [31]. The model followed the first law of thermodynamic, assuming a closed system with homogenous contents behaving as an ideal gas during the compression and exhaust strokes. The AHRR is displayed for each fuel in Figs. 13 and 14, disregarding heat transfer losses.

$$\frac{dQ}{d\theta} = \frac{1}{(\gamma - 1)} V \frac{dP}{d\theta} + \frac{\gamma}{(\gamma - 1)} P \frac{dV}{d\theta} \tag{2}$$

The heat release rates showed two stages across fueling strategies for the tested loads. CDC contained a greater diffusion flame than the RCCI modes, as also observed in Ref. [32], resulting in much lower premixed heat release in comparison to the dual fuel operation. CDC had a shorter mixing time and more regions with locally rich air/fuel ratios. In contrast, the n-butanol allowed for in-cylinder stratification by decreasing the global reactivity of the air/fuel mixture before SOI-2, effectively delaying the premixed flame.

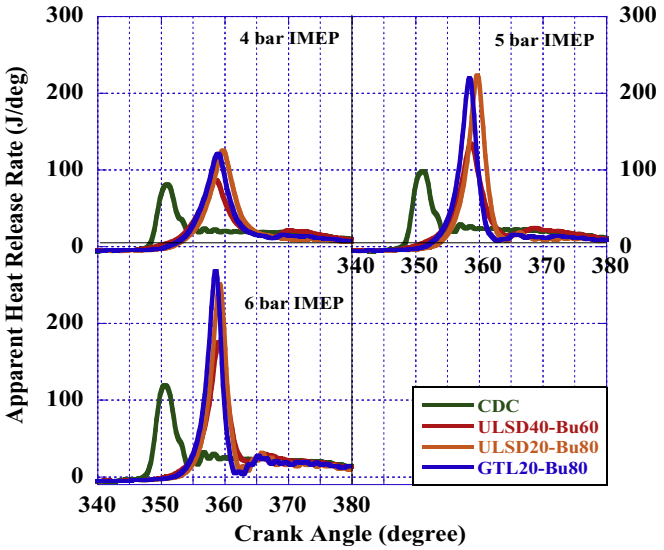

Fig. 13. Apparent Heat Release Rates at 1500 rpm and 4, 5, and 6 bar IMEP.

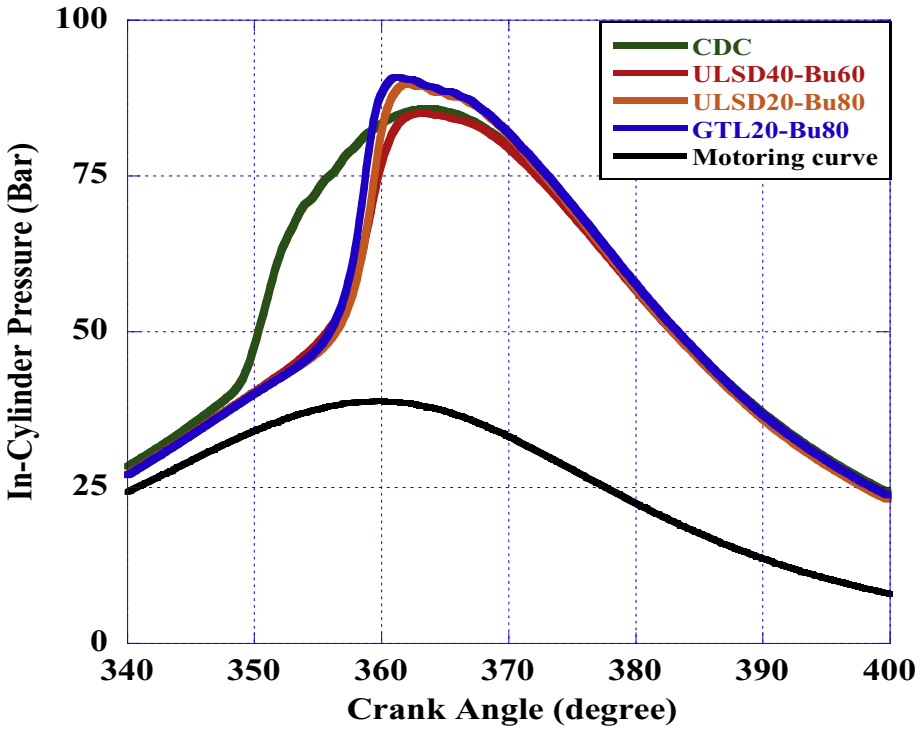

Fig. 12. In-Cylinder Pressure at 1500 rpm and 6 bar IMEP.

Please cite this article in press as: V. Soloiu, et al., Reactivity controlled compression ignition and low temperature combustion of Fischer-Tropsch Fuel Blended with n-butanol, Renewable Energy (2018), https://doi.org/10.1016/j.renene.2018.09.047

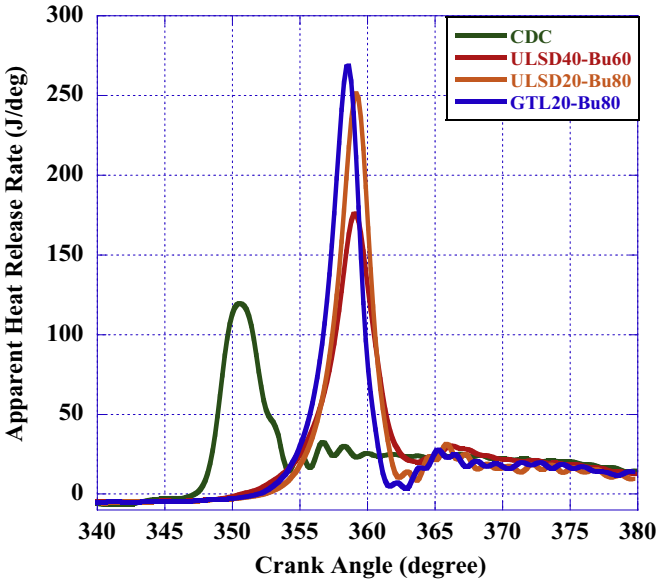

Fig. 14. Apparent Heat Release Rates at 1500 rpm and 6 bar IMEP.

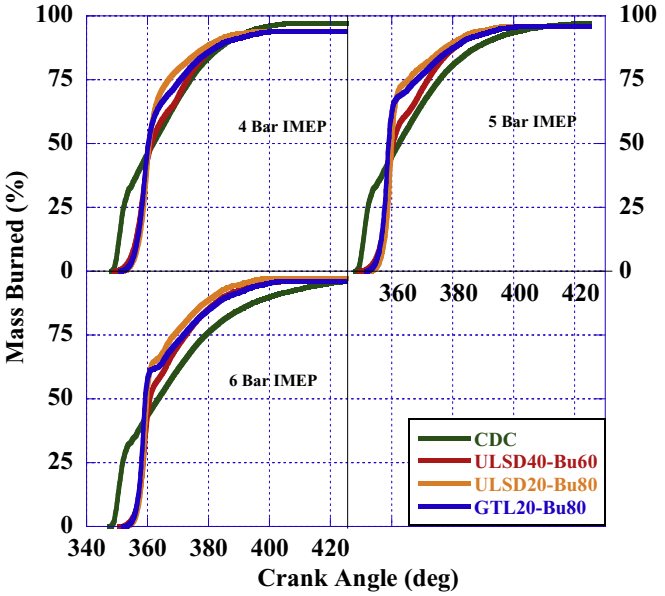

Fig. 15. Mass Burned at 1500 rpm and 4, 5, and 6 Bar IMEP.

More fuel was premixed during dual fuel operation resulting in an evident decrease in diffusion compared to CDC. The magnitude of the diffusion did increase with load as more fuel was available through SOI-2. ULSD40-Bu60 exhibited the largest diffusion at lower load, but at higher loads, the diffusion was comparable across the RCCI modes. In addition, the high latent heat of vaporization of both GTL and n-butanol led to more prominent concave minimums after the premixed phase. This is a result of the SOI-2 event, where the fuel absorbs heat before the start of the diffusion phase.

Compared to ULSD40-Bu60, the peak AHRR increased by 30% at 4 bar and 6 bar IMEP, which can be correlated to the higher SOI-1 mass fraction needed by the reduced cetane number fuel blends. Moreover, the amount of vaporized fuel was higher for the blends due to the high volatility of n-butanol as already observed in the TGA-DTA experiments. Maximum heat release rates were lower for GTL20-Bu80 than ULSD20-Bu80 at the two lower loads. At 6 bar IMEP, however, GTL20-Bu80 had a 10% high peak heat release rate, as seen in Fig. 14, given the differences in SOI-1 mass fraction. The equivalence ratio before SOI-2 for GTL20-Bu80 was higher than ULSD20-Bu80 at higher loads, steadily increasing the overall AHRR. The difference in DCN between ULSD and GTL can also be noted, as GTL20-Bu80 had an earlier maximum AHRR.

6.3. Mass fraction burned

Mass fraction burned was determined through integration of the net heat release rates, which allowed the analysis of combustion phasing and the fuel burn rate. Fig. 15 presents the mass fraction burned across loads for all operated fuels. Crank angles at which 10%, 50%, and 90% of the fuel mass was burned (CA10, CA50, and CA90) were extracted from the curve to determine ignition delay and combustion duration (CD), which are provided in Table 8. Combustion phasing was sustained within 2 CAD of the defined CA50 at 360 CAD. Ignition delay was defined as the period from SOI-1 to CA10, a common definition for ID determination [33], while combustion duration was defined as the period from CA10 to CA90.

The definition for ID, however, did not reflect an accurate comparison between CDC and RCCI due to a 7 CAD difference between CA10 for the operation modes. ID for RCCI was similar for the fuels across the tested loads. The DCN did not have a significant effect on the ID, as combustion phasing was maintained by modulating the mass fractions of SOI-1 and SOI-2 along with constant volumetric efficiency. All three fuels started burning around the same time, ± 0.1 ms, however, the burn rate varies for each fuel halfway through the combustion event. Around CA50, inflections can be observed, refer to Fig. 16, due to SOI-2, which delayed the combustion gradually as the liquid jet produced a cooling effect in the cylinder. The most prominent inflection was observed for

Table 8
Ignition delay and combustion duration across engine loads.

ID/CD (ms)	CDC	ULSD40-Bu60	ULSD20-Bu80	GTL20-Bu80
4 Bar IMEP	1.3/4.0	6.20/3.25	6.3/2.8	6.25/3.3
5 Bar IMEP	1.4/4.6	6.25/3.00	6.4/2.6	6.25/3.0
6 Bar IMEP	1.6/5.6	6.30/3.10	6.4/2.7	6.30/3.3

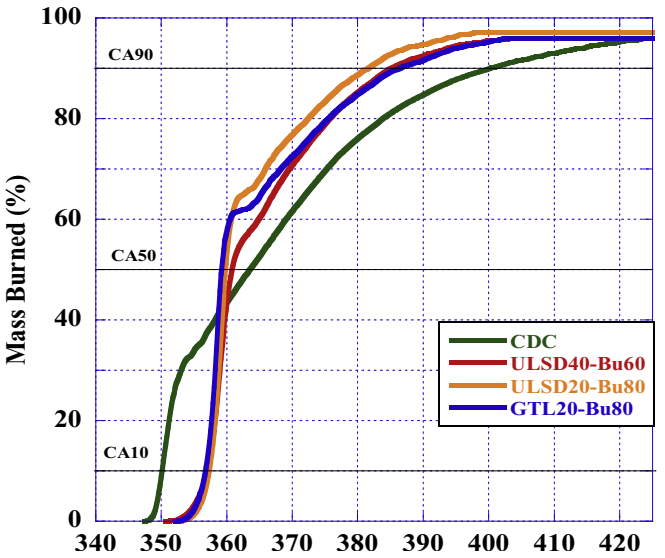

Fig. 16. Mass burned at 6 bar IMEP.

GTL20-Bu80 due to the higher combined latent heat of vaporization of the fuel blend.

Combustion duration for ULSD40-Bu60 was about 1.0 ms−2.5 ms shorter than CDC and further decreases were found for ULSD20-Bu80. Fuels with lower ignition quality are generally beneficial for increasing the amount of the premixed combustion phase through increased mixing time and shorter combustion durations, reducing major losses through heat transfer. ULSD20-Bu80 led to a 15% decrease in combustion duration compared to ULSD40-Bu60 at each load. GTL20-Bu80, however, had a similar CD at lower loads and slightly higher at the highest load compared to ULSD40-Bu60. The GTL blend had a 28% lower DCN than neat ULSD, in which the extended CD can be related to the volatility of the kerosene and smaller droplet sizes which inhibited flame propagation at a lower local equivalence ratio and slower flame speeds [34].

6.4. Instantaneous volume-averaged gas temperature

The in-cylinder combustion temperatures were obtained from the pressure, volumetric efficiency, and linear piston movement, assuming the air/fuel mixture behaves as an ideal gas. As displayed in Fig. 17, peak gas temperatures were below 1600 °C across all loads, achieving low temperature combustion [35]. ULSD40-Bu60 had the lowest combustion temperatures correlating to the trends in the apparent heat release rates.

Maximum in-cylinder temperatures for ULSD20-Bu80 were 25 °C higher than GTL20-Bu80 at the lowest loads, and similar at 6 bar IMEP reaching 1560 °C as observed in Fig. 18. This trend can be attributed to the high volatility and DCN of GTL kerosene compared to ULSD, which advanced the start of heat release and induced higher temperatures at peak compression when operating at 6 bar IMEP. The butanol blends also show an inflection at peak temperatures, correlating to the effect of the liquid jet of SOI-2 entering the combustion chamber. The butanol blends cools the air/fuel mixture through the high heat absorption before continuing the diffusion flame and temperature rise.

6.5. Ringing intensity

The ringing intensity (RI) was determined with Eq. 3 from combustion temperatures, the MPRR, and the maximum in-cylinder pressures. A constant β of 0.05 was used as it is frequently utilized in literature [36] to relate the pressure oscillation amplitude. Fig. 19 displays the RI for the conducted research points, with the n-butanol blends significantly increasing the

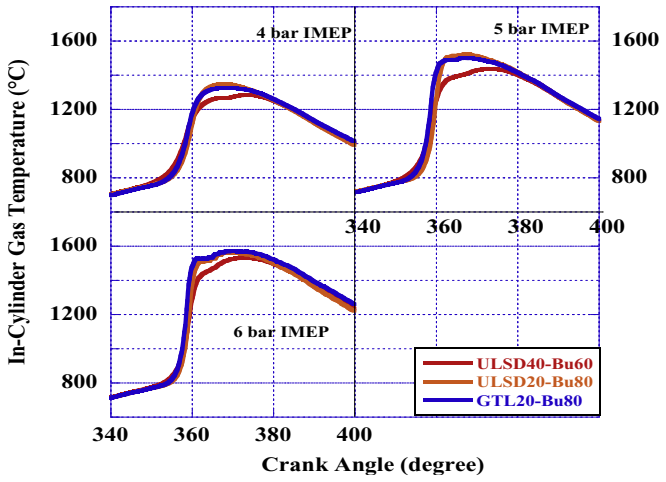

Fig. 17. In-cylinder combustion temperatures at 4, 5, and 6 bar IMEP.

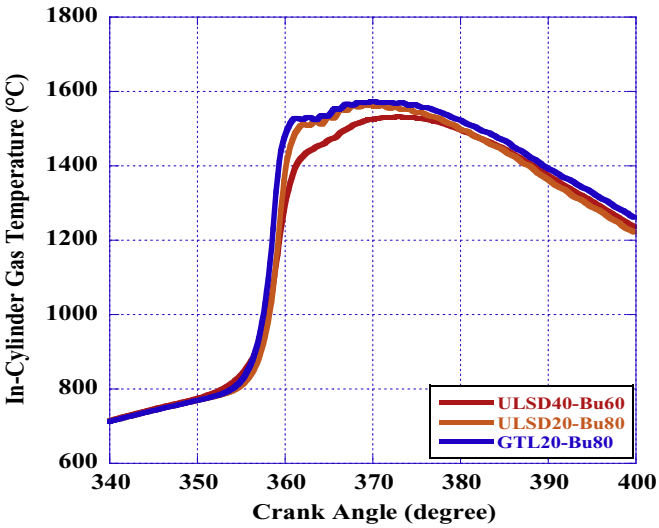

Fig. 18. In-cylinder combustion temperatures at 6 bar IMEP.

values as load increased.

$$RI = \frac{\left(\beta\left(\frac{dP}{dt}\right)_{max}\right)^2}{2\gamma P_{max}}\sqrt{\gamma RT_{max}} \quad (3)$$

RI for ULSD40-BU60 was 30% lower compared to CDC at the lowest load, and 55% higher at 6 bar IMEP. At 4 bar IMEP, the pressure rise and heat release rate was less rapid, which is attributed to an over-lean mixture. Ringing intensity increased up to 80% and 85% for ULSD20-Bu80 and GTL20-Bu80 respectively, compared to CDC. This resulted from increased mass fractions of SOI-1, which affected the reactivity gradient in the cylinder and led to increasingly higher MPRR. This behavior in RI has also been observed by Soloiu et al. [37] as the ratio of n-butanol to diesel in a blend increases.

6.6. Heat flux and Heat Losses

Heat transfer due to convection and radiation were modeled based on a study by Borman and Nishiwaki [38] for the evaluation of heat fluxes and heat transfer losses. The overall heat flux ($\dot{q}$) was determined using Eq. (4), which implemented revisions by Soloiu

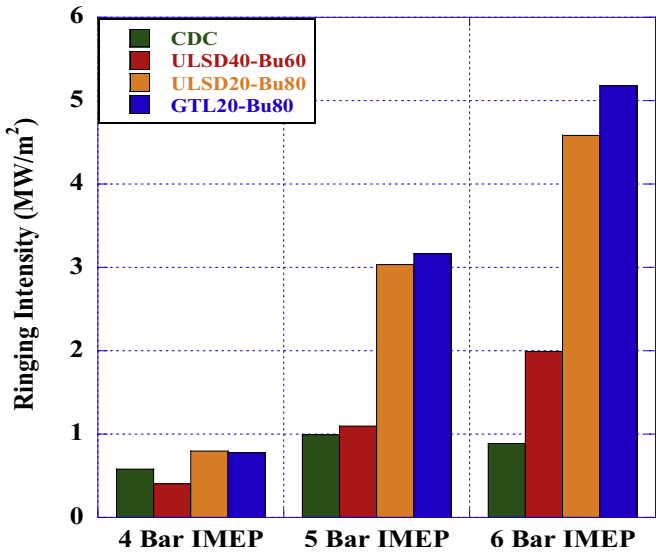

Fig. 19. Ringing intensity across engine loads.

Please cite this article in press as: V. Soloiu, et al., Reactivity controlled compression ignition and low temperature combustion of Fischer-Tropsch Fuel Blended with n-butanol, Renewable Energy (2018), https://doi.org/10.1016/j.renene.2018.09.047

[39]. The model assumed a uniform wall temperature (T_w) and used empirical constants along the air thermal conductivity (λ_A) and combustion temperatures (T_A). The model also required calculation of Reynolds Number (*Re*) as determined using Eq. 5 [40]. The models identified heat transfer from the direct contact of in-cylinder gases to the walls and liner in the form of convection as well as radiation due to heat transfer from the high temperature diffusion flames and particulate matter [41]. The heat fluxes for RCCI and CDC are displayed in Fig. 20.

$$\dot{q}(\alpha) = A\frac{\lambda_A(\alpha)}{D}Re^{0.7}(T_A(\alpha) - T_w) + \sigma * \varepsilon\left(T_A^4(\alpha) - T_W^4\right) \quad (4)$$

$$Re(\alpha) = \rho(\alpha)\frac{S*N*D}{30\mu(\alpha)} \quad (5)$$

Maximum convection flux was 10% higher for the GTL and ULSD blends compared to CDC and 7% higher in relation to ULSD40-BU60. The higher peak values are attributed to the higher SOI-1 mass fraction and higher combustion temperatures. The presence of n-butanol affected the local droplet temperatures and vapor pressures due to characteristic higher vaporization rate as observed in the TGA-DTA, increasing convection fluxes. Peak radiation flux can be observed to increase up to 22% for the butanol blends in comparison to ULSD40-Bu60 and CDC. Magnitudes can correlate with the diffusion identified in the AHRR, where GTL20-Bu80 and ULSD20-Bu80 were shown with the lowest inflection between premixed and mixing-controlled combustion. The radiation flux followed the in-cylinder temperature curve with a delay due to the nature of heat transfer to the surrounding walls.

The determined convection and radiation heat transfer were related to net heat release in order to identify relative magnitude of the losses in relation to the total fuel energy. Fig. 21 represents the energy balance for the blended RCCI operations at 6 bar IMEP, which takes into account the heat transfer in addition to fuel evaporation and crevice flows. Blow-by and crevice were considered to account for 2% of the total fuel energy release. GTL20-Bu80 had a lower net heat release fraction compared to ULSD20-Bu80, which is attributed to the larger cooling effect of GTL compared to ULSD. Both butanol-blended RCCI modes have 5% radiation losses; however, the improved atomization quality of GTL20-Bu80 reduced convection losses by 1.5% compared to ULSD20-Bu80. Combustion inefficiencies were 4% for the GTL blend and 3% for the ULSD blend as shown in the area above the radiation loss. Relatively high combustion efficiencies were achieved for RCCI mode as a result of low temperature combustion.

7. Emissions and efficiencies

7.1. Nitrogen oxides and soot

The effect of a reduced cetane number on combustion was reflected in the brake specific emissions. The analysis focused on the tradeoff between NOx and soot as well as combustion inefficiencies reflected by CO and UHC. Trends in NOx are the result of the local cylinder temperatures and fuel chemistry in the LTC regime. Fig. 22 illustrates the NOx emissions where the RCCI modes with port fuel injected n-butanol resulted in a homogeneous air/fuel mixture prior to ignition, resulting in much lower levels compared to CDC. The slight change in trend for n-butanol blends can be related to some increases seen in AHRR, 30%–40% higher than neat ULSD RCCI, which increased local temperatures and promoted more NOx emissions. Overall, the ULSD40-Bu60 decreased NOx levels by 90% and 70% at 4 and 6 bar IMEP, respectively, compared to CDC. While the direct injection at SOI-1 mass fraction started to converge for

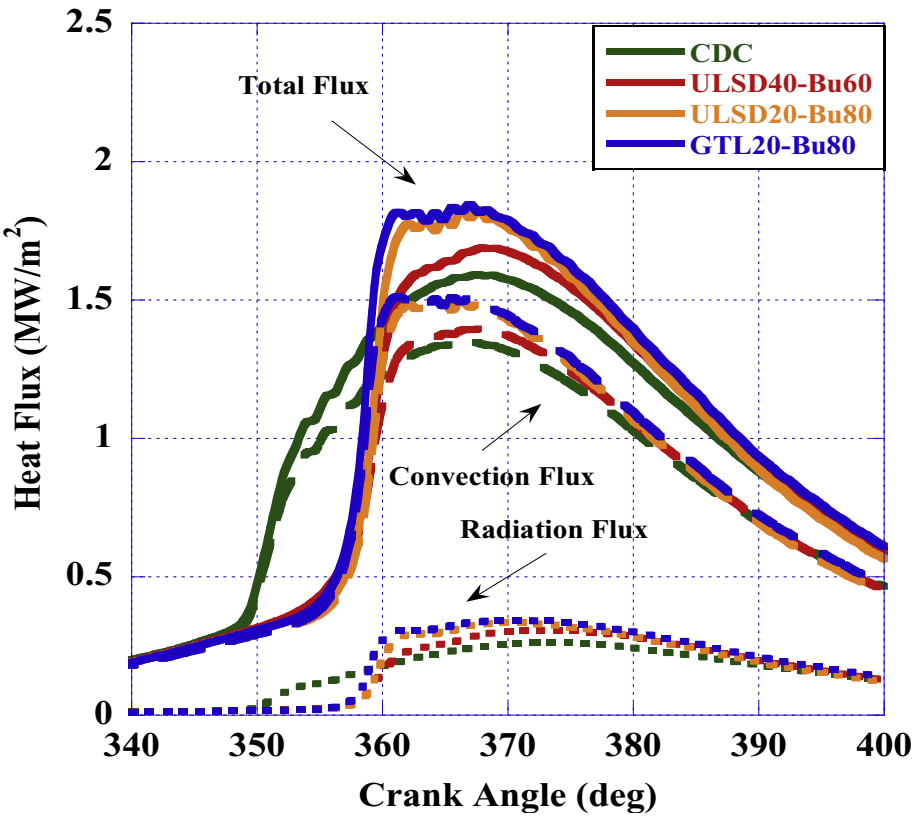

Fig. 20. Heat flux at 6 bar IMEP.

Please cite this article in press as: V. Soloiu, et al., Reactivity controlled compression ignition and low temperature combustion of Fischer-Tropsch Fuel Blended with n-butanol, Renewable Energy (2018), https://doi.org/10.1016/j.renene.2018.09.047

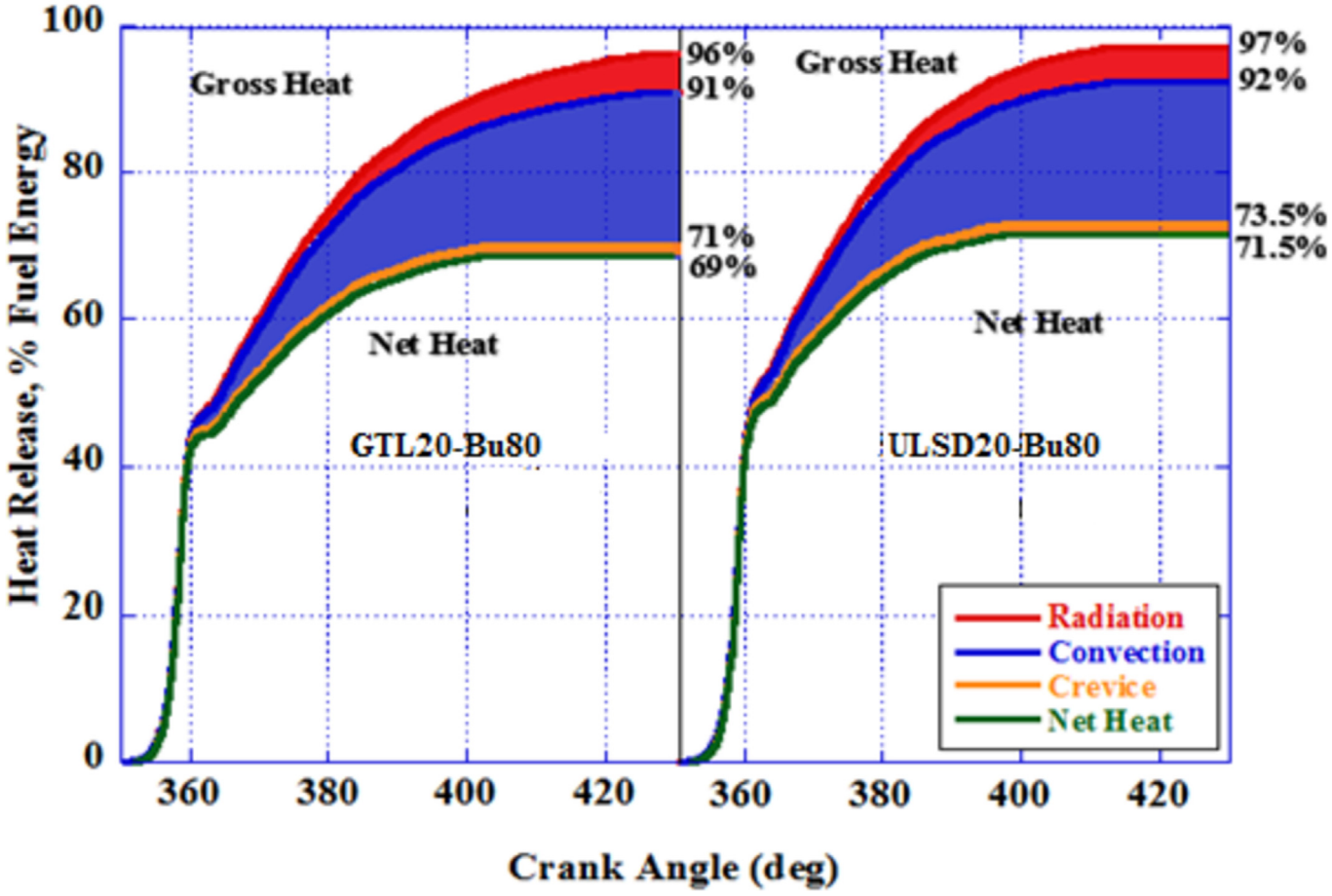

Fig. 21. Heat losses for GTL20-Bu80 and ULD20-Bu80 at 6 bar IMEP.

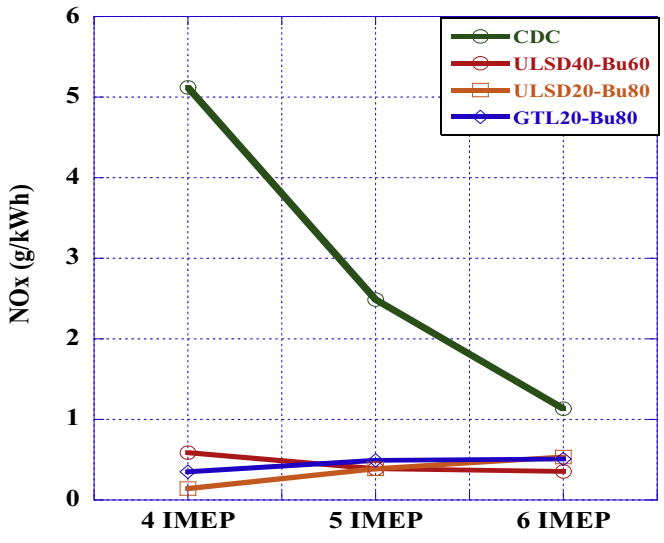

Fig. 22. NOx emissions across engine loads.

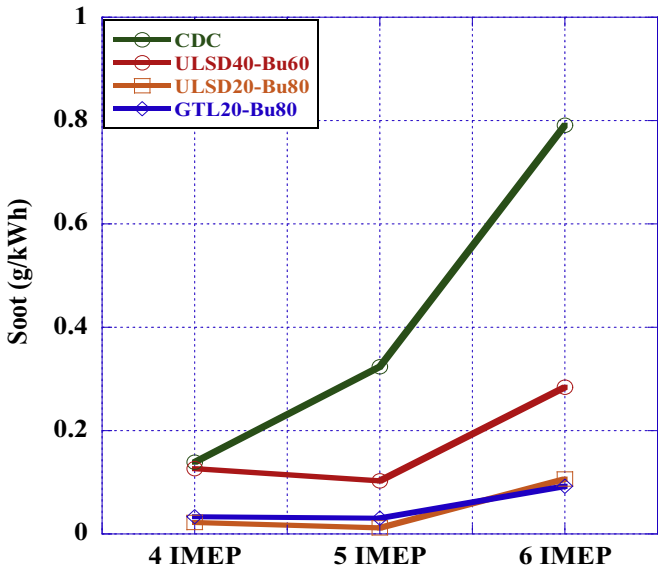

Fig. 23. Soot emissions across engine loads.

both n-butanol blends as load increased, the higher levels of NOx for GTL20-Bu80 were caused from the higher mass fraction of SOI-2 at the two lower loads, creating more pockets of stoichiometric air/fuel ratios.

Fig. 23 displays the indicated specific soot emissions which were reduced by 65% by neat RCCI and by 90% by both n-butanol blends RCCI in comparison to CDC. The split DI and early PFI allowed for in-cylinder blending which created a more homogenous mixture, reducing rich areas across the chamber. The higher oxygen content provided by n-butanol allowed a more complete combustion, enhancing soot oxidation also found by Refs. [42,43], and led to

Please cite this article in press as: V. Soloiu, et al., Reactivity controlled compression ignition and low temperature combustion of Fischer-Tropsch Fuel Blended with n-butanol, Renewable Energy (2018), https://doi.org/10.1016/j.renene.2018.09.047

significant reductions for the n-butanol blends in RCCI compared to ULSD40-Bu60. The lower DCN of the fuel blends increased the mass fraction of SOI-2, allowing more fuel to premix prior to ignition. At the lower loads, the soot levels for GTL20-Bu80 increased by 40–60% in relation to ULSD20-Bu80. This is correlated with the lower maximum AHRR observed for the GTL blends at lower loads and higher at 6 bar IMEP, where the carbon recession rate increases with higher mixing rates [44].

7.2. Carbon monoxide, unburned hydrocarbons, and aldehydes

Indicated specific CO and UHC trends are illustrated in Fig. 24. The two higher loads had a reduction in CO levels when compared to results at 4 bar IMEP. UHC levels decreased as load increased for RCCI, indicating improved combustion stability. At 4 bar IMEP, over-lean regions (relative air/fuel ratio at 4.5) combined with LTC induced the highest CO levels across loads, as CO was unable to be oxidized [45]. CO emissions were lower by 25% for the butanol blends compared to ULSD40-Bu60. Better mixture homogeneity resulted from increased volatility of the direct injected butanol blends. This can be considered as the driving factor given the CO levels for n-butanol blends nearly overlaid each other and were lower overall compared to ULSD40-Bu60.

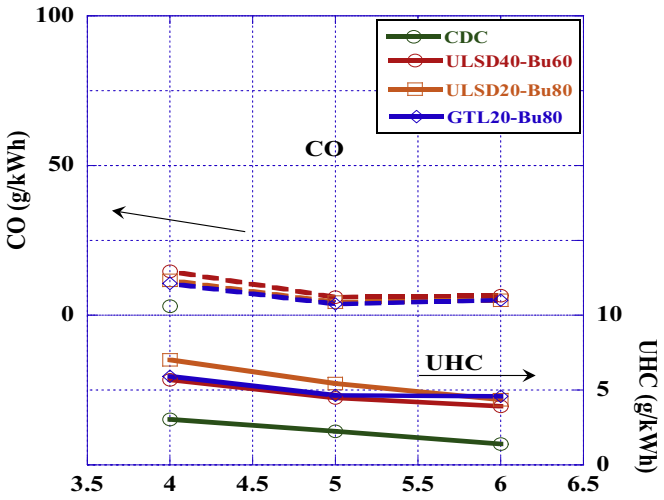

Fig. 24. CO and UHC emissions across engine loads.

UHC emissions were 55–70% lower for CDC as a result of lower crevice flow and wall impingement compared with the earlier injection timings of RCCI that would promote those phenomena. Compared to ULSD40-Bu60, RCCI with the GTL blend increased UHC levels 10–20% as a result of the longer SOI-1 durations, with increased spray penetration inducing wall wetting and crevice effects. ULSD20-Bu80 had higher levels of UHC compared to GTL20-Bu80 at the lower loads, where injection duration was shorter for the GTL blend. In contrast, at the highest load, GTL20-Bu80 had higher relative UHC production and longer injection duration.

Additionally, Fig. 25 shows that the aldehyde emissions, although unregulated, have been found as a consequence of using alcohol for binary mixtures and in-cylinder blending confirmed in Ref. [46] as well. Compared to single fuel injection, ULSD40-Bu60 increased aldehyde emissions by 80–85%, increasing further with the n-butanol blends. The butanol blends had the highest aldehyde emissions correlating to quenching effects and trapped mass in the piston fireland and crevice flow seen in also in Ref. [47]. Increase in convection flux for GTL20-Bu80 at 6 bar IMEP, as observed in the heat transfer analysis, can be related to the increase in aldehyde levels and related quenching effects.

7.3. Efficiencies

The mechanical and indicated thermal efficiencies (ITE) are presented in Fig. 26. Mechanical efficiencies for both ULSD RCCI modes were 3%–4% higher than CDC and GTL20-Bu80. ULSD20-Bu80 lead to slightly longer ignition delays and shorter combustion durations, increasing the useful energy due to larger reductions in heat transfer losses in respect to the researched RCCI modes. Mechanical efficiencies were lowest for GTL20-Bu80

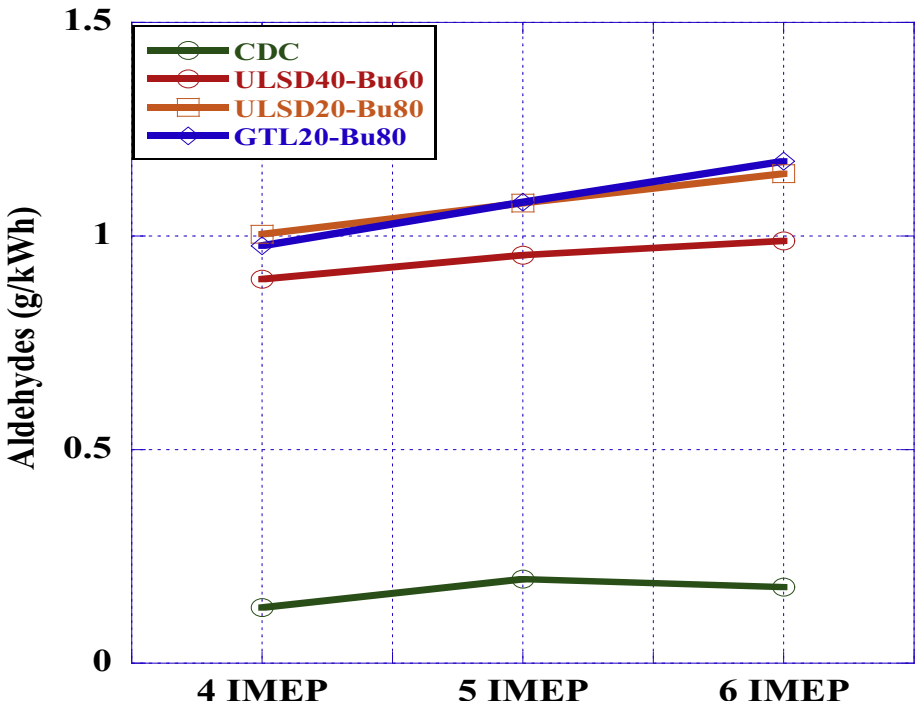

Fig. 25. Aldehyde emissions across engine loads.

Please cite this article in press as: V. Soloiu, et al., Reactivity controlled compression ignition and low temperature combustion of Fischer-Tropsch Fuel Blended with n-butanol, Renewable Energy (2018), https://doi.org/10.1016/j.renene.2018.09.047

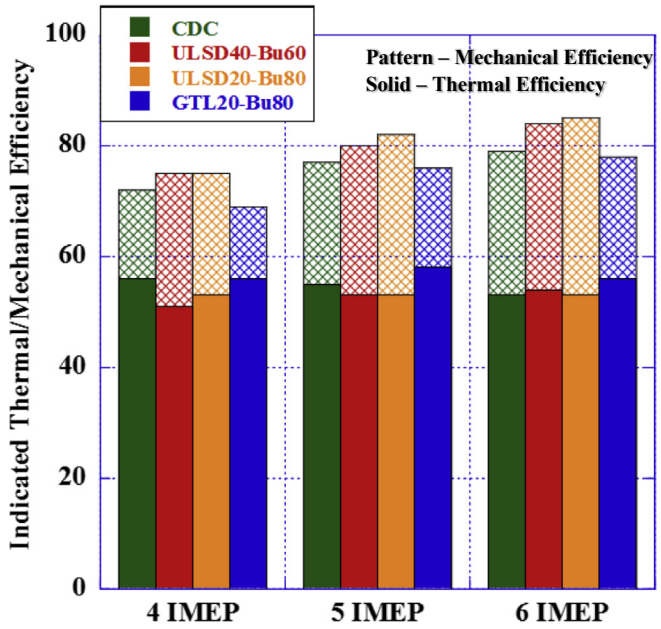

Fig. 26. Indicated thermal and mechanical efficiency.

because of the high pressure rise rates and the earlier onset of ignition, reducing the useful work during the power stroke. ULSD20-Bu80 had higher mechanical efficiencies at the two higher loads compared to ULSD40-Bu60 due to the larger increase in combustion pressures and heat release rates as load increased.

With the supercharger and high pressure injection pump externally driven, CDC and RCCI modes resulted in indicated thermal efficiencies above 50% across loads with GTL20-Bu80 reaching 58% at 4 bar IMEP. Higher ITE for GTL RCCI is attributed to the larger difference in fuel density in relation to energy density compared to ULSD and the ULSD-butanol blend. ITE reduced in CDC as load increased because of undermixing and reductions in combustion efficiency.

Fig. 27 presents the diesel equivalent brake specific fuel consumption (BSFC) taking into account the differences in fuel density and lower heating value. BSFC for conventional diesel combustion was relatively constant across loads. Dual fuel combustion resulted in reductions as load increased, corresponding to the increases in mechanical efficiency. The energy density of the high reactivity fuels was equivalent to that of conventional diesel; however, the lower energy density of n-butanol increased BSFC between 23% and 33% in RCCI compared to CDC. GTL20-Bu80 had the highest BSFC compared to the other dual fuel modes given the low fuel density of neat GTL.

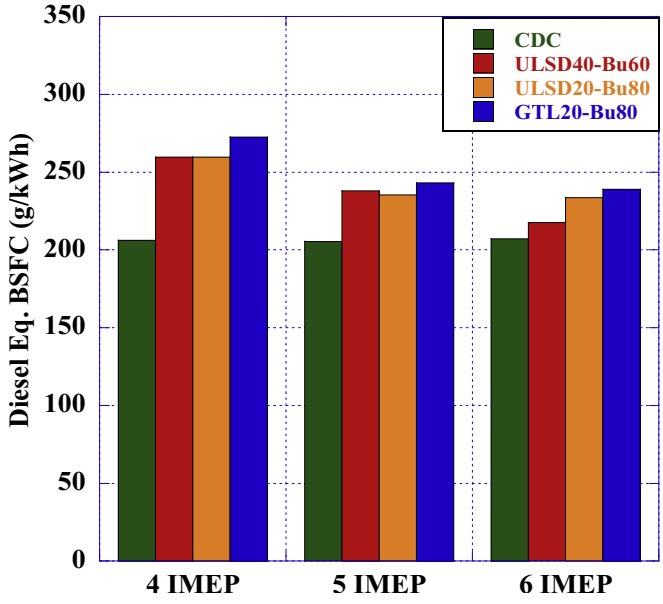

Fig. 27. Diesel equivalent brake specific fuel consumption.

8. Conclusions

RCCI and dual fuel low temperature combustion research was conducted in a single-cylinder experimental compression ignition engine at 1500 rpm across loads from 4 to 6 bar IMEP. Combustion has been investigated with fuel blends of n-butanol compared to neat ULSD to increase control of combustion by reducing the ignition quality. Butanol was blended with either ULSD or Fischer Tropsch synthetic paraffinic kerosene (GTL) at a ratio of 50% by mass (ULSD20-Bu80 and GTL20-Bu80), resulting in reductions in the cetane number by 40% and 28% respectively, compared to neat ULSD. A constant 60% by mass PFI fraction of n-butanol was implemented across operating points for all RCCI modes and the combustion phasing (CA50) was maintained at TDC by varying the mass fraction of the split DI events at 60° BTDC and TDC. RCCI delayed ignition by 7 CAD compared to conventional diesel combustion, resulting in a sharper rise in pressure. All RCCI modes had similar ignition delay; however, increases in the mass fraction of SOI-1 for the reduced cetane number fuels increased peak pressures and the maximum pressure rise rates (MPRR). MPRR exceeded the general accepted limit of 15 bar/deg for the low cetane number fuels. Peak apparent heat release rates for RCCI with the butanol blends increased by 30% at each load increment. The difference in peak heat release rates for the GTL-butanol and ULSD-butanol blends are directly related to the differences in the mass fraction of SOI-1. Combustion duration was reduced between 1.0 ms and 2.5 ms for RCCI compared to CDC. The GTL blend exhibited a shorter ignition delay and longer combustion duration compared to the ULSD blend as a result of the higher volatility, reducing local equivalence ratios and flame speeds. Low temperature combustion was achieved through RCCI across each load. The butanol blends increased ringing intensity drastically higher than CDC and neat ULSD RCCI.

All RCCI modes reduced both NOx and soot up to 90%. Differences in NOx levels for the butanol blends are directly related to the maximum heat release rates. The higher oxygen content of port fuel injected butanol enhanced soot oxidation for all RCCI modes and further reductions were found for the butanol blends. CO and UHC emissions increased for RCCI compared to CDC. The combination of over-lean regions and low temperature combustion at the lowest load resulted in the largest CO emissions. CO was reduced by 25% for both butanol blends compared to neat ULSD in RCCI, correlating to the additional butanol as the driving factor. The relationship between the fuels and UHC was found to be correlated to the mass fraction of SOI-1, affecting spray penetration and wall wetting. Aldehyde emissions increased by over 80% in RCCI compared to CDC. Increases for the butanol blends are a result of quenching effects and trapped mass in the piston fireland. Mechanical efficiencies increased 3–4% in RCCI compared to CDC. The GTL-butanol blend had the lowest mechanical efficiencies in RCCI, as a result of the more rapid heat release rate, causing reductions in the useful work during the power stroke. The diesel equivalent brake specific fuel consumption was relatively constant across loads for CDC, however reduced with load in RCCI. Increases in BSFC for RCCI were

Please cite this article in press as: V. Soloiu, et al., Reactivity controlled compression ignition and low temperature combustion of Fischer-Tropsch Fuel Blended with n-butanol, Renewable Energy (2018), https://doi.org/10.1016/j.renene.2018.09.047

a result of the lower energy density of butanol. *N*-Butanol blended with either ULSD or Fischer Tropsch synthetic paraffinic kerosene (GTL) proved to be optimal in RCCI mode, achieving low temperature combustion along with desirable emission characteristics and maintained engine power.

Acknowledgments

This paper is based upon work supported by the National Science Foundation under Grant No. 1609524. The authors would like to acknolwedge the contribution of the Air Force Research Laboratory for supplying the experimental fuel, Mike Smith of Exergy Engineering LLC for the custom injector nozzle, Janusz Waszkielewicz and Charles McGuffey from PAC for CID 510, Daniel Stockton from AVL for technical support, Mathew Viele of Vieletech, Joseph Wolfgang of Malvern, Samuel Olesky from Kistler, Mastry Engine Center LLC and Sophia Fleri from GSU.

Abbreviations

AHRR	apparent heat release rate
ATDC	after top dead center
BSFC	brake specific fuel consumption
BTDC	before top dead center
CA10	crank angle for 10% mass fraction burned
CA50	crank angle for 50% mass fraction burned
CA90	crank angle for 90% mass fraction burned
CAD	crank angle degree
Cd	combustion delay
CD	combustion duration
CDC	conventional diesel combustion
CN	cetane number
CO	carbon monoxide
COV	coefficient of variation
CVCC	constant volume combustion chamber
DAQ	data acquisition
DI	direct injection
DTA	differential thermal analysis
Dv (10)	largest droplet size of 10% fuel spray
Dv (50)	largest droplet size of 50% fuel spray
Dv (90)	largest droplet size of 90% fuel spray
EGR	exhaust gas recirculation
F-T	Fischer Tropsch
GTL	gas-to-liquid
GTL20-Bu80	dual fuel combustion with 60% butanol PFI and 40% GTL blend DI
HCCI	homogeneous charge compression ignition
HCHO	formaldehyde
ID	ignition delay
IMEP	indicated mean effective pressure
ITE	indicated thermal efficiency
LHV	lower heating value
LTC	low temperature combustion
MPRR	maximum pressure rise rate
NOx	nitrogen oxides
NTC	negative temperature coefficient
PCCI	premixed charge compression ignition
PFI	port fuel injection
PM	particulate matter
RCCI	reactivity controlled compression ignition
Re	Reynolds number
RI	ringing intensity
rpm	rotations per minute
SMD	Sauter mean diameter
SOI-1	start of the first injection
SOI-2	start of the second injection
TA10	temperature at which 10% of the fuel vaporized
TA50	temperature at which 50% of the fuel vaporized
TA90	temperature at which 90% of the fuel vaporized
TDC	top dead center
TGA	thermogravimetric analysis
ULSD20-Bu80	dual fuel combustion with 60% butanol PFI and 40% ULSD blend DI
ULSD40-Bu60	dual fuel combustion with 60% butanol PFI and 40% neat ULSD DI
UHC	unburned hydrocarbons
ULSD	ultra-low sulfur diesel

Appendix A. Instrument Accuracy

Table 9
Measurement Accuracies for Selected Measurements.

Instrument	Measured Parameter	Accuracy
TQ513 Torque Sensor	Torque	±0.06%
Meriam Z50MC2-2 Laminar Flow Meter	Air Mass Flow Rate	±0.72%
213 Max Flow Meter	Common Rail Fuel Flow Rate	±0.2%
P001 Max Flow Meter	PFI Fuel Flow Rate	±0.2%
Kistler 6053 cc Piezoelectric Pressure Transducer	In-Cylinder Pressure	±0.19%
EMS Model 5002	Intake/Exhaust CO_2	±0.3%
AVL SESAM FTIR V4	NO_x concentration	±2.2%
	CO_2 concentration	±1.6%
	CO concentration	±1.6%
	HC concentration	±2.2%
	HCHO concentration	±2.2%
AVL 483 Micro Soot Sensor	Soot Concentration	±3.8%

References

[1] J. Bacha, J. Freel, A. Gibbs, et al., Diesel Fuels Technical Review, Chevron Products Company, 2007.
[2] V. Prikhodko, S. Curran, T. Barone, S. Lewis, et al., Emission characteristics of a diesel engine operating with in-cylinder gasoline and diesel fuel blending, SAE Int. J. Fuels Lubr. 3 (2) (2010) 946–955, https://doi.org/10.4271/2010-01-2266.
[3] K. Pohlkamp, R. Reitz, Reactivity Controlled Compression Ignition (RCCI) in a Single-Cylinder Air-cooled HSDI Diesel Engine, 2012, https://doi.org/10.4271/2012-32-0074. SAE Technical Paper 2012-32-0074.
[4] X. Han, M. Zheng, J. Tjong, T. Li, Suitability Study of N-Butanol for Enabling PCCI and HCCI and RCCI Combustion on a High Compression-ratio Diesel Engine, 2015, https://doi.org/10.4271/2015-01-1816. SAE Technical Paper 2015-01-1816.
[5] V. Soloiu, R. Gaubert, J. Moncada, et al., Partially Premixed Compression Ignition of Fischer Tropsch Synthetic Paraffinic Kerosene (S8) with PFI of N-butanol, ASME Internal Combustion Engine Division, 2017. ICEF2017–3674.
[6] D. DelVescovo, S. Kokjohn, R. Reitz, The effects of charge preparation, fuel stratification, and premixed fuel chemistry on reactivity controlled compression ignition (RCCI) combustion, SAE Int. J. Eng. 10 (4) (2017).
[7] H. Wang, D. DelVescovo, M. Yao, R. Reitz, Numerical study of RCCI and HCCI combustion processes using gasoline, diesel, iso-butanol and DTBP cetane improver, SAE Int. J. Eng. 8 (2) (2015) 831–845, https://doi.org/10.4271/2015-01-0850.
[8] R. Michikawauchi, S. Tanno, Y. Ito, M. Kanda, Combustion improvement of diesel engine by alcohol addition - investigation of port injection method and blended fuel method, SAE Int. J. Fuels Lubr. 4 (1) (2011) 48–57, https://doi.org/10.4271/2011-01-0336.
[9] S.L. Kokjohn, R.M. Hanson, D.A. Splitter, R.D. Reitz, Experiments and modeling of dual-fuel HCCI and PCCI combustion using in-cylinder fuel blending, SAE Int. J. Eng. 2 (2) (2009) 24–39.
[10] S.L. Kokjohn, R.M. Hanson, D.A. Splitter, R.D. Reitz, Fuel reactivity controlled compression ignition (RCCI): a pathway to controlled high-efficiency clean combustion, Int. J. Engine Res. 12 (3) (2011) 209–226.
[11] K. Wadumesthrige, K. Ng, S. Salley, Properties of butanol-biodiesel-ULSD ternary mixtures, SAE Int. J. Fuels Lubr. 3 (2) (2010) 660–670, https://

Please cite this article in press as: V. Soloiu, et al., Reactivity controlled compression ignition and low temperature combustion of Fischer-Tropsch Fuel Blended with n-butanol, Renewable Energy (2018), https://doi.org/10.1016/j.renene.2018.09.047

doi.org/10.4271/2010-01-2133.
[12] O. Doğan, The influence of n-butanol/diesel fuel blends utilization on a small diesel engine performance and emissions, Fuel 90 (7) (2011) 2467–2472.
[13] P. Dürre, Biobutanol: an attractive biofuel, Biotechnol. J. 2 (2007) 1525–1534.
[14] Z. Şahin, O.N. Aksu, Experimental investigation of the effects of using low ratio n-butanol/diesel fuel blends on engine performance and exhaust emissions in a turbocharged DI diesel engine, Renew. Energy 77 (2015) 279–290.
[15] United States Department of Agriculture, Closing in on butanol fuel, Agric. Res. (2014) 8.
[16] S. Gürgen, B. Ünver, İ. Altın, Prediction of cyclic variability in a diesel engine fueled with n-butanol and diesel fuel blends using artificial neural network, Renew. Energy 117 (2018) 538–544.
[17] S.S. Gill, A. Tsolakis, K.D. Dearn, J. Rodríguez-Fernández, Combustion characteristics and emissions of Fischer–Tropsch diesel fuels in IC engines, Prog. Energy Combust. Sci. 37 (4) (2011) 503–523.
[18] P. Schaberg, I. Myburgh, J. Botha, I. Khalek, Comparative Emissions Performance of Sasol Fischer-tropsch Diesel Fuel in Current and Older Technology Heavy-duty Engines, 2000, https://doi.org/10.4271/2000-01-1912. SAE Technical Paper 2000-01-1912.
[19] C. Moses, Comparative Evaluation of Semi-synthetic Jet Fuels, U.S. Air Force Research Laboratories, New Braunfels, Texas, 2008.
[20] T. Alleman, R. McCormick, Fischer-tropsch Diesel Fuels - Properties and Exhaust Emissions: a Literature Review, 2003, https://doi.org/10.4271/2003-01-0763. SAE Technical Paper 2003-01-0763.
[21] A. Nayyar, D. Sharma, S. Lal Soni, A. Mathur, Characterization of n-butanol diesel blends on a small size variable compression ratio diesel engine: modeling and experimental investigation, Energy Convers. Manag. 150 (2017) 242–258.
[22] C. Atkinson, G. Thompson, M. Traver, N. Clark, In-Cylinder Combustion Pressure Characteristics of Fischer-tropsch and Conventional Diesel Fuels in a Heavy Duty CI Engine, 1999, https://doi.org/10.4271/1999-01-1472. SAE Technical Paper 1999-01-1472.
[23] K. Kitano, S. Misawa, M. Mori, I. Sakata, et al., GTL Fuel Impact on DI Diesel Emissions, 2007, https://doi.org/10.4271/2007-01-2004. SAE Technical Paper 2007-01-2004.
[24] A. Piperel, L. Pidol, L. Noel, N. Jeuland, Influence of Fischer-tropsch Incorporation on Engine Outputs and Performances of a Modern Diesel Engine with Standard and Optimized Settings, 2011, https://doi.org/10.4271/2011-24-0114. SAE Technical Paper 2011-24-0114.
[25] A. Abu-Jrai, J. Rodríguez-Fernández, A. Tsolakis, A. Megaritis, K. Theinnoi, K, R.F. Cracknell, R.H. Clark, Performance, combustion and emissions of a diesel engine operated with reformed EGR. Comparison of diesel and GTL fuelling, Fuel 88 (2009).
[26] M. Lapuerta, R. Garcia-Contreras, J. Campos-Fernandez, M. Pilar Dorado, Stability, lubricity, viscosity, and colf-flow properties of alcohol-diesel blends, Energy Fuels 24 (2010) 4497–4502.
[27] Alternative Fuels Data Center – Fuel Properties Comparison, October 29, 2014, 2014, Oct 29 [cited 2017 Nov 5]. Available from: www.afdc.energy.gov.
[28] ASTM D7668-14a, Standard Test Method for Determination of Derived Cetane Number (DCN) of Diesel Fuel Oils—ignition Delay and Combustion Delay Using a Constant Volume Combustion Chamber Method, ASTM International, West Conshohocken, PA, 2014.
[29] D. Kim, J. Martz, A. Violi, Effects of fuel physical properties on direct injection spray and ignition behavior, Fuel 180 (2016) 481–496.
[30] V. Soloiu, J.D. Moncada, R. Gaubert, M. Muiños, S. Harp, M. Ilie, A. Zdanowickz, G. Molina, LTC (low-temperature combustion) analysis of PCCI (premixed charge compression ignition) with n-butanol and cotton seed biodiesel versus combustion and emissions characteristics of their binary mixtures, Renew. Energy, doi:10.1016/j.renene.2018.02.061.
[31] J. Heywood, Internal Combustion Engine Fundamentals, McGraw-Hill Companies, New York, NY, 1988.
[32] Z. Chen, J. Liu, Z. Wu, C. Lee, Effects of port fuel injection (PFI) of n-butanol and EGR on combustion and emissions of a direct injection diesel engine, Energy Convers. Manag. 76 (2013) 725–731.
[33] U. Joshi, Z. Zheng, A. Shrestha, N. Henein, E. Sattler, An investigation on sensitivity of ignition delay and activation energy in diesel combustion, J. Eng. Gas Turbines Power 137 (9) (2015), 091506-091506-8.
[34] S. Yousuffuddin, Effect of combustion duration on the operating and performance characteristics of hydrogen-ethanol dual fueled engine: an experimental analysis, Int. J. Adv. Autom. Technol. 1 (1) (2017) 36–45.
[35] G. Neely, S. Sasaki, Y. Huang, J. Leet, et al., New Diesel Emission Control Strategy to Meet US Tier 2 Emissions Regulations, 2005. SAE Technical Paper 2005-01-1091, https://doi.org/10.4271/2005-01-1091.
[36] J.A. Eng, Characterization of Pressure Waves in HCCI Combustion, 2002, https://doi.org/10.4271/2002-01-2859. SAE Technical Paper 2002-01-2859.
[37] V. Soloiu, M. Muinos, S. Harp, Investigation of Dual Fuel PCCI (PFI of N-Butanol and DI-ULSD) Compared with DI of Binary Mixtures of the Same Fuels in an Omnivorous Diesel Engine, 2015. SAE Technical Paper 2015-01-0857, https://doi.org/10.4271/2015-01-0857.
[38] G. Borman, K. Nishiwaki, Internal-combustion engine heat transfer, Prog. Energy Combust. Sci. 13 (1987) 1–46.
[39] V. Soloiu, M. Duggan, S. Harp, B. Vlcek, D. Williams, PFI (port fuel injection) of n-butanol and direct injection of biodiesel to attain LTC (low-temperature combustion) for low-emissions idling in a compression engine, Energy 52 (2013) 143–154.
[40] V. Soloiu, J. Lewis, Y. Yoshihara, K. Nishiwaki, Combustion characteristics of a charcoal slurry in a direct injection diesel engine and the impact on the injection system performance, Energy 36 (7) (2011) 4353.
[41] J. Benajes, J. Martín, A. García, et al., In-cylinder soot radiation heat transfer in direct-injection diesel engines, Energy Convers. Manag. 106 (2015) 414–427.
[42] F. Zhao, W. Yang, W. Yu, H. Li, Y.Y. Sim, T. Liu, K.L. Tay, Numerical study of soot particles from low temperature combustion of engine fueled with diesel fuel and unsaturation biodiesel fuels, Appl. Energy 211 (2018) 187–193.
[43] M. Mofijur, M.G. Rasul, J. Hyde, A.K. Azad, R. Mamat, M.M.K. Bhuiya, Role of biofuel and their binary (diesel–biodiesel) and ternary (ethanol–biodiesel–diesel) blends on internal combustion engines emission reduction, Renew. Sustain. Energy Rev. 53 (2016) 265–278.
[44] C.A. Amman, D.L. Stivender, S.L. Plee, J.S. MacDonald, Some rudiments of diesel particulate emissions, SAE paper 800251, SAE Trans. 89 (1980).
[45] M. Wissink, R.D. Reitz, Direct dual fuel stratification, a path to combine the benefits of RCCI and PPC, SAE Int. J. Eng. 8 (2) (2015) 878–889.
[46] B. Choi, X. Jiang, Y.K. Kim, G. Jung, C. Lee, I. Choi, C.S. Song, Effect of diesel fuel blend with n-butanol on the emission of a turbocharged common rail direct injection diesel engine, Appl. Energy 146 (2015) 20–28.
[47] CIMAC WG 17, Gas engines. Methane and formaldehyde emissions of gas engines. CIMAC Position Paper WG 17, 2014.

Please cite this article in press as: V. Soloiu, et al., Reactivity controlled compression ignition and low temperature combustion of Fischer-Tropsch Fuel Blended with n-butanol, Renewable Energy (2018), https://doi.org/10.1016/j.renene.2018.09.047